

## REPORT DOCUMENTATION PAGE

AFRL-SR-AR-TR-06-0035

The public reporting burden for this collection of information is estimated to average 1 hour per response, including 1 gathering and maintaining the data needed, and completing and reviewing the collection of information. Send comments information, including suggestions for reducing the burden, to the Department of Defense, Executive Services and Com. that notwithstanding any other provision of law, no person shall be subject to any penalty for failing to comply with a collection of information if it does not display a valid control number.

PLEASE DO NOT RETURN YOUR FORM TO THE ABOVE ORGANIZATION.

1. REPORT DATE (DD-MM-YYYY) 14/08/2005	2. REPORT TYPE Final Technical report	3. DATES COVERED (From - To) 15/08/2000 thru 14/08/2005		
4. TITLE AND SUBTITLE  "Analytic Hyperspectral Sensing"		5a. CONTRACT NUMBER F49620-00-C-0040		
		5b. GRANT NUMBER		
		5c. PROGRAM ELEMENT NUMBER		
6. AUTHOR(S)  Dr. Ronald R. Coifman		5d. PROJECT NUMBER		
		5e. TASK NUMBER		
		5f. WORK UNIT NUMBER		
7. PERFORMING ORGANIZATION NAME(S) AND ADDRESS(ES) Plain Sight Systems, Inc 1020 Sherman Avenue Hamden, CT 06514		8. PERFORMING ORGANIZATION REPORT NUMBER 0002-5 Research Data Item		
9. SPONSORING/MONITORING AGENCY NAME(S) AND ADDRESS(ES) AF Office of Scientific Research 4015 Wilson Boulevard, Room 713 Arlington, VA 22203-1954		10. SPONSOR/MONITOR'S ACRONYM(S) USAF, AFRL		
		11. SPONSOR/MONITOR'S REPORT NUMBER(S)		
12. DISTRIBUTION/AVAILABILITY STATEMENT "Any opinions, findings and conclusions or recommendations expressed in this material are those of the author and do not necessarily reflect the views of the Defense Advanced Research Projects Agency"				
13. SUPPLEMENTARY NOTES  <i>Approved for public release distribution unlimited</i>				
14. ABSTRACT In the last year (no-cost extension), Plain Sight Systems reached the goal of successfully building its second NIR standoff hyperspectral imaging system, NSTIS, the Near-Infrared Spectral Target Identification System. Data collection and development of associated analysis tools took place, and progress was made in the use of NSTIS as an integrated sensing and processing platform in collaboration with our initial customer (Lockheed Martin). In concert with development of the NSTIS systems, Plain Sight Systems continued to develop spectrally tunable MOEMS based light sources and associated algorithms for direct spectral feature measurements via collaboration with Yale University and Kansas State University. These were and continue to be applied in real time chemical imaging tasks such as diagnostic pathology.				
15. SUBJECT TERMS				
16. SECURITY CLASSIFICATION OF: a. REPORT U b. ABSTRACT U c. THIS PAGE U		17. LIMITATION OF ABSTRACT	18. NUMBER OF PAGES 54	19a. NAME OF RESPONSIBLE PERSON Dr. Ronald R. Coifman 19b. TELEPHONE NUMBER (Include area code) (203) 248-8534

# **“Analytic Hyperspectral Sensing”**

## **Final Technical Report**

August 14, 2005

Air Force Office of Scientific Research

**Contract #: F49620-00-C-0040**

Dr. Ronald R. Coifman  
Plain Sight Systems, Inc.  
(novated from F.M.A.& H. Corporation)  
1020 Sherman Avenue  
Hamden, CT 06514  
(203) 248-8212

“Any opinions, findings and conclusions or recommendations expressed in this material are those of the author and do not necessarily reflect the views of the Defense Advanced Research Projects Agency”

# AIR FORCE OFFICE OF SCIENTIFIC RESEARCH

08 FEB 2006

Page 1 of 2

## DTIC Data

---

Purchase Request Number: FQ8671-0001043

**BPN:**

**Proposal Number:** 00-NM-075

**Type Submission:** New Work Effort

**Inst. Control Number:** F49620-00-C-0040DEF

**Institution:** PLAIN SIGHT SYSTEMS, INCORPORATED

**Primary Investigator:** Dr. Ronald R. Coifman

**Invention Ind:** none

**Project/Task:** K3040 / 0

**Program Manager:** Dr. Arje Nachman

---

**Objective:**

The objective is to produce a hyperspectral sensing system which is both substantially faster and more discriminating than any currently proposed or available.

**Approach:**

The approach envisions an integration of modern wavelet signal processing and arrays of micromechanical/optoelectronic devices. The wavelets processing engine would provide the system with the ability to filter (both temporally and spatially) in almost real time so that the data burden currently hobbling the hyperspectral sensors (a cube of raw data which is interrogated after collection) can be avoided. The filtering (a version of high dimensional inner products) will communicate with the devices (in one realization with an array of micro mirrors) so that digestible displays are produced. Earlier, one dimensional work by the PI, upgraded the acquisition radar for the Longbow missile system.

**Progress:**

**Year:** 2004    **Month:**

PROGRESS REPORT: F49620-00-C-0040    FROM: 15 AUG 02 TO 14 AUG 03

In the last year, Plain Sight Systems (P55) has concentrated efforts on moving existing designs into the InfraRed region, but has also pursued algorithm implementation and Graphical User Interface (GUI) software, Digital Mirror Device (DMD) driving refinements including new pseudo-random-Walsh based multiplexing modalities, and a general effort to field the prototype that was described in previous reports moving the prototype out of the lab and into other indoor and outdoor locations for data collection efforts. The Infra Red effort has involved design and specification of a system incorporating almost all common off-the-shelf (COTS) components, as well as another improved design incorporating custom optical components specifically designed for Near InfraRed (NIR) operation, and with the specifics of the present system in mind. Plain Sight Systems has procured most of the components for these systems, and is in the process of refining the design, and finalizing the last few components. This effort is expected to lead to the construction of prototypes over the next half to ? of a year.

**Year:** 2005    **Month:** 02

ANNUAL REPORT FOR: F49620-00-C-0040

In the last year, Plain Sight Systems have concentrated efforts on building, testing, and refining designs from the previous year for a system operating in the Near Infrared (NIR) region. We have also continued to pursue algorithm implementation and graphical user interface(GUI) software and Digital Micro-mirror Device (DMD)driving refinements including newer pseu do-random wavelet based multiplexing modalities. As a result, we were able to field a prototype that was capable of being tripod mounted and along with a standard computer, could be moved out of the lab and into other indoor and outdoor locations for a successful realistic field data collection efforts.

# AIR FORCE OFFICE OF SCIENTIFIC RESEARCH

---

08 FEB 2006

DTIC Data

Page 2 of 2

---

## Progress:

**Year:** 2006    **Month:** 02    **Final**

Final report for F49620-00-C-0040

In the last year (no-cost extension), Plain Sight Systems reached the goal of successfully building its second NIR standoff hyperspectral imaging system, NSTIS, the Near-Infrared Spectral Target Identification System. Data collection and development of associated analysis tools took place, and progress was made in the use of NSTIS as an integrated sensing and processing platform inc collaboration with our initial customer (Lockheed Martin). In concert with development of the NSTIS systems, Plain Sight Systens continued to develop spectrally tunable MOEMS based light sources and associated algorithms for direct spectral feature measurements via collaboration with Yale University and Kansas State University. These were and continue to be applied in real time chemical imaging tasks such as diagnostic pathology.

**Date:** August 15, 2005

**Performer:** Plain Sight Systems Inc.

**Contract#:** F49620-00-C-0040

**Title:** "Analytic Hyperspectral Sensing"

**PI:** Dr. Ronald R. Coifman

(203) 248-8534

#### **Other Team Members:**

Stanford subcontract

Drs. D. Miller, J. Harris, O. Solegaard

Yale subcontract

Dr. F. Warner

Three LC subcontract

Drs. W. Fateley, R. Hammaker

**Program Director:** Dr. Arje Nachman

AFOSR/NM (703) 696-8427

---

#### **Project Goals**

The overall goal of the project was to demonstrate the feasibility of portable MOEMS based hyperspectral imaging systems, and to provide real time detection and chemical surveillance capabilities, by tuning the data collection process to the desired chemical information.

#### **Approach**

We have pursued, through feasibility and prototype construction phases,

- A digital mirror array (DMA) based still hyperspectral processing camera permitting direct extraction of spatio-spectral features from a scene of interest.
- Mirror modulating algorithms to enable video rate detection.
- Other spatial light modulators capable of processing on the sensor, including grating light modulators, arrays of optical switches, and others capable of operating in various infrared wavelength regions.
- Digitally controlled optical sensors.

#### **Accomplished Milestones**

By the beginning of this last contract year, Plain Sight reached the goal of successfully building its first NIR standoff hyperspectral imaging system, NSTIS, the Near-Infrared Spectral Target Identification System. In concert with development of the first NSTIS, spectrally tunable MOEMS based light sources and associated algorithms for direct spectral feature measurements were developed via collaboration with Yale University and Kansas State University. These were and continue to be applied in real time chemical imaging tasks such as diagnostic pathology.

During the no-cost extension, as part of this contract and in conjunction with cost sharing and other funding sources, Plain Sight assembled the second NSTIS, performed and supported data collection and development of associated analysis tools, and made progress in the use of NSTIS

as an integrated sensing and processing platform in collaboration with our initial customer (Lockheed Martin).

## Future Milestones

- Continued testing with Lockheed and also a new customer - the Marine Battle Labs
- Optimization of NSTIS and movement into the mid-infrared with other SLMs
- Portable MEMS based hyperspectral system capable of video rate chemometry
- Optical switch synaptic systems for optical data processing on the sensor

## Demonstration Activity

- Coded aperture spectrograph.
- Spatio/spectral target detection.
- Spectral tuned light generation.
- Tunable broadband filtering.
- Multifunctional spectrometry.
- Direct chemometric modes.

## Remarks

Our goal was to have a prototype portable demonstration field device capable of a variety of hyperspectral image acquisition modes when fitted with appropriate optical attachments. *This goal has been achieved for the visible and near infrared wavelength regions.* We have also finished the development of a second and improved near infrared version of the initial DMA based system that demonstrates improved image quality. Furthermore, we are now in a position to propose and build a third generation system capable of demonstrating 1) higher optical performance and throughput, 2) faster frame rates, 3) greater portability, and 4) without loss of performance, the ability to simultaneously analyze two wavelength regions or to supply a second channel for broadband imaging for the purpose of targeting and motion tracking.

## Technical approach and resource allocation on the project

In this final (no-cost extension) phase, the effort concentrated on data collection, hardware drivers, design and prototyping of instrumentation around the DMA by Plain Sight Systems. No work was performed by subcontractors during this phase.

# Coded Aperture Spectrograph Status Report

## Summary

We have constructed and tested novel prototype passive hyperspectral imaging systems based on the modality of replacing the slit of an imaging spectrograph with a Digital Micromirror Array or Device (DMA or DMD). The advantages of this novel configuration include the ability to scan with the DMA, rather than by macro-mechanical motion of the camera relative to the target of interest, and the ability to collect data in an adaptively multiplexed way.

In the final 2 years, Plain Sight Systems concentrated efforts on building, testing, and refining designs for a system operating in the Near Infrared (NIR) region. We have also continued to pursue algorithm implementation and GUI software, and DMD driving refinements including newer pseudo-random wavelet based multiplexing modalities. As a result, we were able to field two prototypes operating in the NIR region that were capable of being tripod mounted and, along with a standard computer, could be moved out of the lab and into other indoor and outdoor locations for successful realistic field data collection efforts. One of these systems was successfully tested at a military facility (China Lake NAVAIR) and was subsequently delivered to a contractor (Lockheed Martin) for further evaluation and development. The second system is to be scheduled for demonstration at another military facility (Marine Battle Labs) during 2006.

The fielding of the first NIR system originally involved the design and specification of a system incorporating almost all COTS components with the exception of some that were recoated for the NIR spectral range. However, replacing some of the COTS design with an optical configuration invented in house outside the scope of this contract, we were able to overcome difficulties of the NIR region and some of the major design challenges of using the DMA in an imaging system. Also, by analyzing collected data and refining the existing design, we were able to gain valuable experience that has led to the refinement of the design and the build of a similar second NIR system.

## Optical Concept

This spectral imaging system is based on a dispersive imaging spectrograph layout as shown in Figure 1. In conventional imaging spectrographs, the entrance aperture is a vertical rectangular slit. Typically one must translate the image across the width of the slit. We have replaced the typical entrance slit with a DMD aperture where the DMD is also at the focal plane of an F-mount (Nikon) or FD-mount (Canon) camera lens. The target “object” is focused onto the DMD and is scanned into the imaging spectrograph system using programmable aperture encoding methods. In conventional raster scanning modality, a rectangular subset of DMD mirrors that is orthogonal to the dispersive dimension of the imaging spectrograph is selected to sequentially illuminate the subsequent optical system. This effects a spatial scanning of a single entrance slit allowing that portion of the image on the DMD to enter the optical system. The spatial dislocation in the dispersion axis of the optics affects an angular difference in the incident rays upon the grating. This results in a translation of the spatio-spectral image at the focal plane of the array detector. Scanning the image can be accomplished using Hadamard or a combination of Hadamard and Raster scanning.

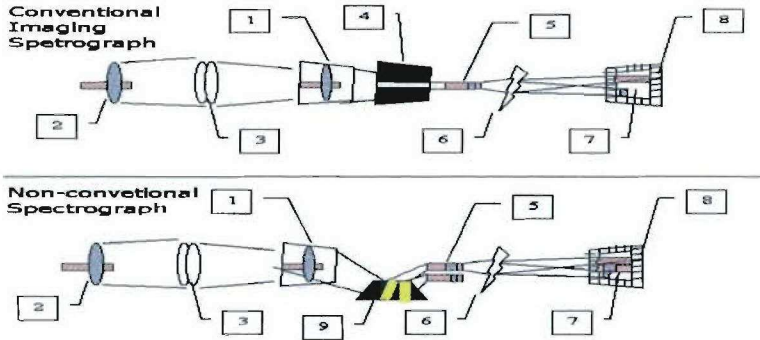


**Figure 1:** Dispersive imaging spectrograph layout and modifications: In the conventional imaging spectrograph, an incoming image (1) of a scene to be analyzed (2), is focused, by a lens (3), onto a plane mask which contains a single horizontal slit (4). In this way, a one-dimensional horizontal slice (5) through the original image (1) passes through the mask (4). A dispersion device (6) disperses vertically the slice-image (5). The result is that each point in the slice-image (5) is dispersed into a vertical spectrum of the light at that point. This results in a 2D spectrograph image (7). The spectrograph image (7) is re-imaged by optics (not shown) onto a detector array (8). A hyper-spectral image of a scene is obtained by then scanning, one height at a time, across the scene (e.g. from top to bottom). This is typically done by actually moving the apparatus with respect to the scene, or, alternatively, with a scanning mirror. In the modified configuration, a spatial light modulator (9), such as a TI DMD is used in place of the mask (4). In this way, the multiplex advantage is available to the system. Also, scanning can be accomplished electronically, without the need for relative motion of the device with respect to the scene, nor the need for macro-moving parts.

## Development Timeline

### **1<sup>st</sup> system (with imSpector, on optical bench) (project start → 9/2001)**

This compact system demonstrated replacement of mechanical scanning with DMD scanning, and provided early demonstrations of the multiplex advantage. System artifacts were severe, and the system alignment unstable. The device was not usable beyond these simple demonstrations that the concept had merit.

This early system was based on an active light design, in which the DMD is illuminated with broadband light, which is then re-imaged through the sample, into a modified imaging spectrograph. The spectrograph modification consists of removing the entrance slit and placing the sample to sit at the plane formerly occupied by the slit. There were actually 2 distinct embodiments of this setup. Figure 2 shows one of them.

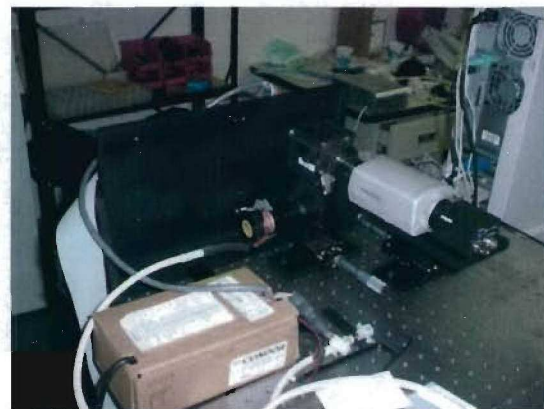


**Figure 2:** Photo of early system.

### **2<sup>nd</sup> System (with imSpector™ and prism, on optical bench) (9/2001 → 12/2001)**

In this iteration, a TIR prism assembly was used to fold the optical path, enabling an optical benchtop prototype that was stable enough to collect data over a period of time. This system was used to demonstrate the adaptive multiplex advantage, and demonstrated the feasibility and merit of making a portable prototype. Figure 3 shows this system.

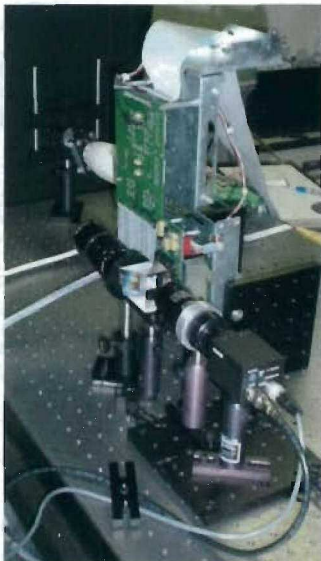


**Figure 3:** Photo of 2<sup>nd</sup> early system, and some data collected while imaging a plant leaf.

### 3<sup>rd</sup> System (with grating and gen1) (1/2002 → 7/2002)

This iteration was intended to be a portable prototype based on the previous system, but the imSpector™ was replaced by a grating, in order to allow flexible choice of gratings for selection of wavelength ranges, and to better characterize the dependence of system performance on component choices. The system is shown uncovered in Figure 4.

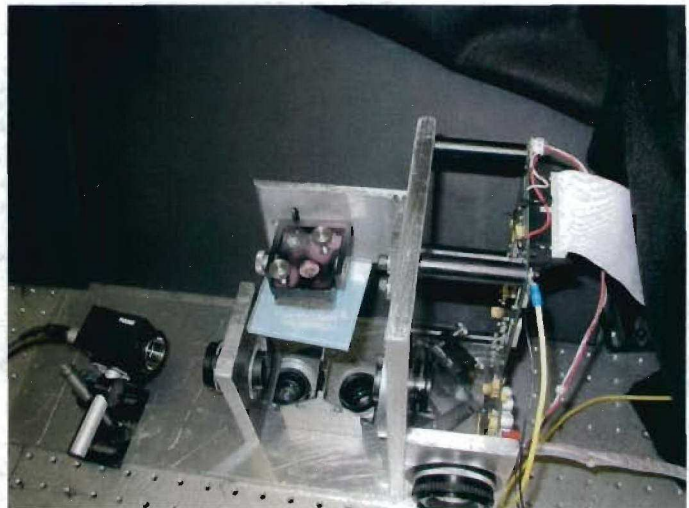


**Figure 4:** Photos of 3<sup>rd</sup> system uncovered.

#### 4th Generation: Fielding the Portable Visible Integrated System (7/2002 → 9/2003)

In this iteration, Plain Sight concentrated on imaging scenes with natural or typical light such as sunlight, room light, and other standard electrical lighting. Other iterations had used laboratory-controlled lighting. Also, this year we characterized the efficacy of our system in a portable mode. This amounted to placing the now-covered camera housing on a rolling cart, together with a PC equipped with a flat-panel display for compactness, and a long extension cord.

We also updated the system software to allow reliable acquisitions at 15 to 20 frames per second, where before this had been a peak rate that was not reliably achieved. This helped us to mitigate the effects of moving cloud cover and other typical phenomena associated with outdoor imaging. Another line of development involved customized pseudo-random multiplex codes. These codes allowed us to mitigate a number of artifacts that had been reported in the previous years' developments. We were able to collect quality datacubes from ordinary objects using a variety of indoor and outdoor lighting conditions.



**Figure 5:** Views of 4<sup>th</sup> generation system mounted on rolling cart.

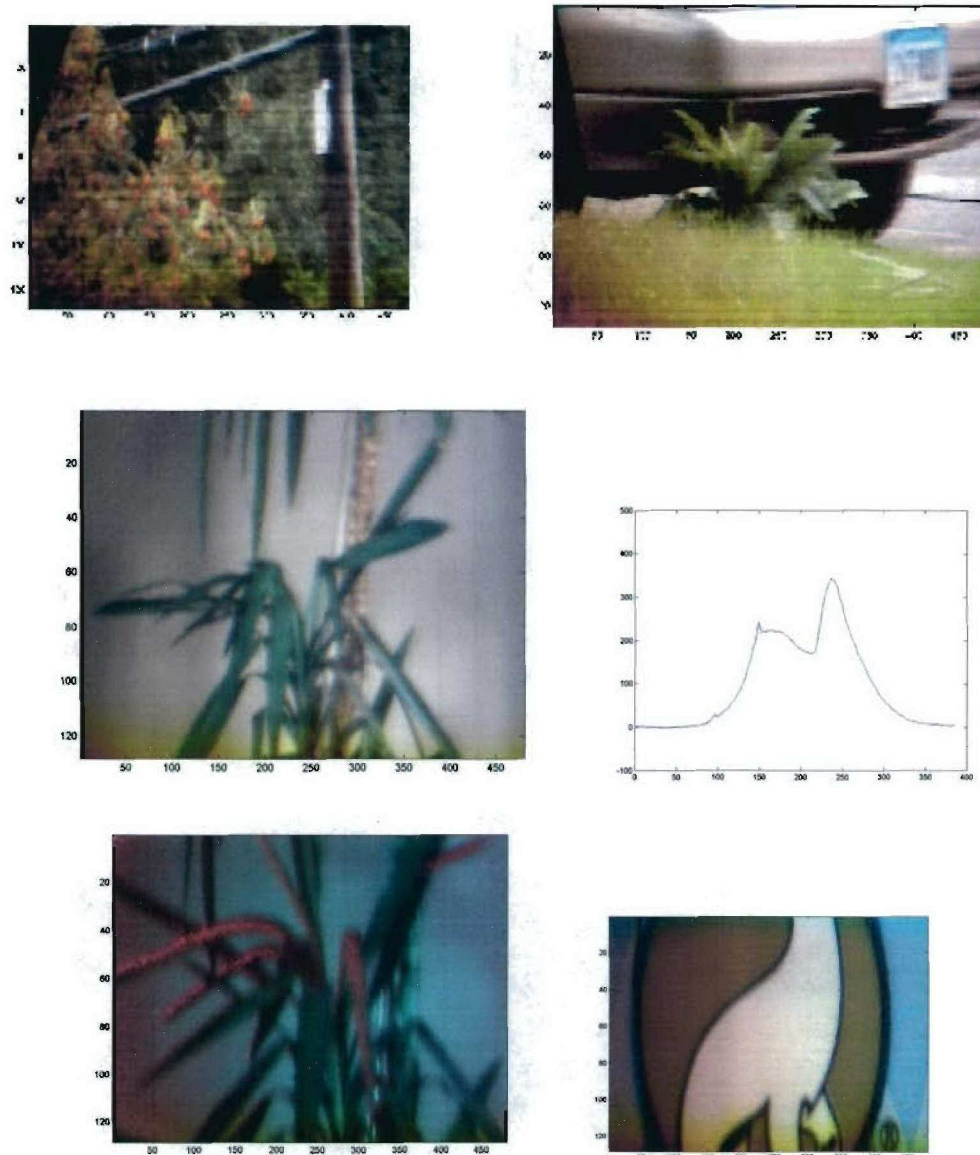


**Figure 6:** Various spectra and pseudo-colored images of data collected by the system.

## Near Infrared System (12/2002 → Present)

In the past year, Plain Sight successfully built its first NIR hyperspectral camera prototype, NSTIS, the Near-Infrared Spectral Target Identification System. It operates by the same fundamental principles as our previous visible wavelength range device, SLM-based multiplexing with no macro-moving parts, but its design was enhanced to allow it to operate in the 900nm to 1700nm region.



**Figure 7:** Several views, electronics exposed, of the NSTIS camera. The leftmost shows the system from the front; center view from the back; rightmost from the side.

### NSTIS Specifications:

Spectral Sampling	1.5625nm
Spectral Resolution	<10nm
Working F#	< 5.6
Typical Data Collection Time	10 sec / datacube
Datacube Dimensions	up to 512x512x532

### NSTIS Components:

- **Housing** – The NSTIS housing consists of custom made, black-painted aluminum parts. The fully assembled system is a non-rectangular shape that fits roughly into a size of 24" wide X 16" High x 21" Deep.
- **Optics** – NSTIS contains custom-mounted optical components designed for operation at F#'s no less than F5.6. These are delicate, precision aligned components and are not user serviceable. The internal custom relay lenses meet the proposed target design specifications: Object diagonal of 12.309mm (tilted object creates a reduced extent for lens design), Min. working distance of 36mm, Mag 1.47, MTF 15 lp/mm at 40%, F# 2.44, Distortion less than 0.5%, Transmission greater than 80% over operational bandwidth, Vignetting less than 5%, Wavelength range 900nm – 1700nm, AR coating R less than 1.5% over spectral range and at marginal ray angles, Chromatic aberrations less than 5 microns, Minimum back focal length: 100 mm, "Telecentric like" performance in

object space. The system fore optic (mounted on the front of the system) is a Canon-mounted lens system. Any standard Canon manual FD-mount lens may be used.

- **DMD & DMD Controller** – NSTIS contains an 848X600 TI DLP chip (DMD) and a custom controller electronics controller board.
- **Camera** – NSTIS includes an Indigo Phoenix™ large-area InGaAs camera, with RTIE electronics.
- **Software & System Controller** – NSTIS is controlled via a Windows XP based computer (HP workstation xw4100 or equivalent), and includes a National instruments PCI-1422 Digital frame grabber, and a Cyber Research CYINT 32P controller board. The system is fully configured for use, and should require no user service.
- **Power Requirements** – 120V 60Hz AC power, rated for at least 20 Amps.

The key attributes of this NIR hyperspectral imaging system are its modular design based on COTS parts with no macro-moving parts, multiplexed data collection for increased sensitivity and frame rates, and the capability of adaptable measurement schemes which make the prototype a promising platform for integrated sensor processing (ISP).

The following figures illustrate and describe the basic optical path of the system.

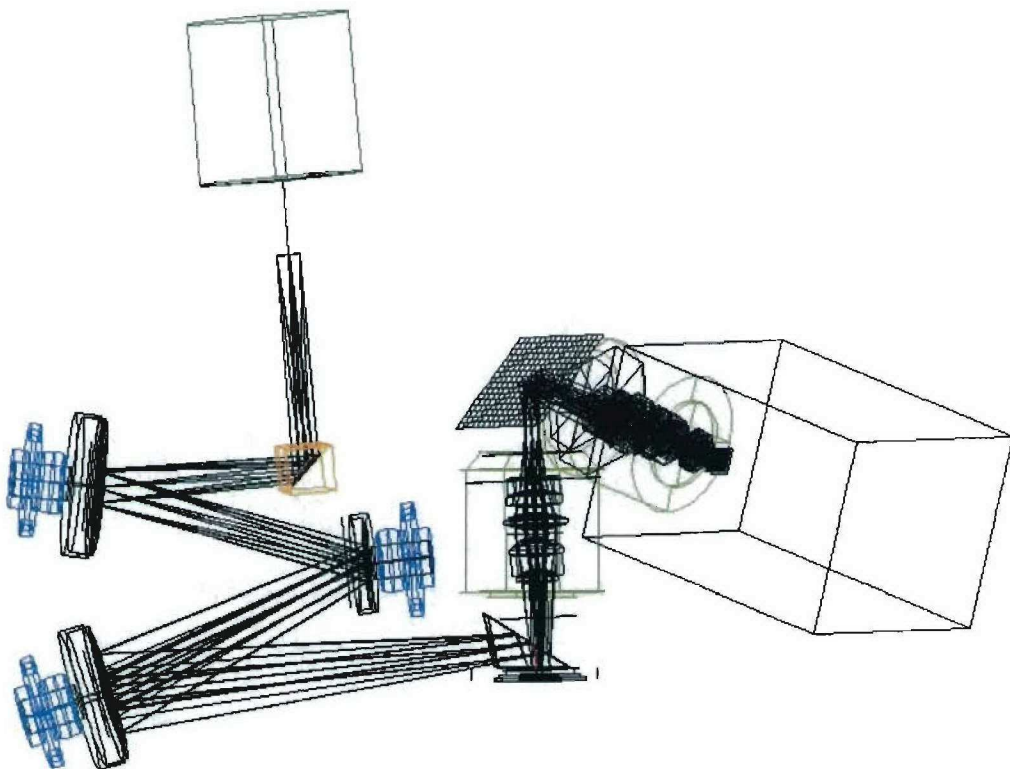


**Figure 8:** NSTIS optical path and layout with ray trace.

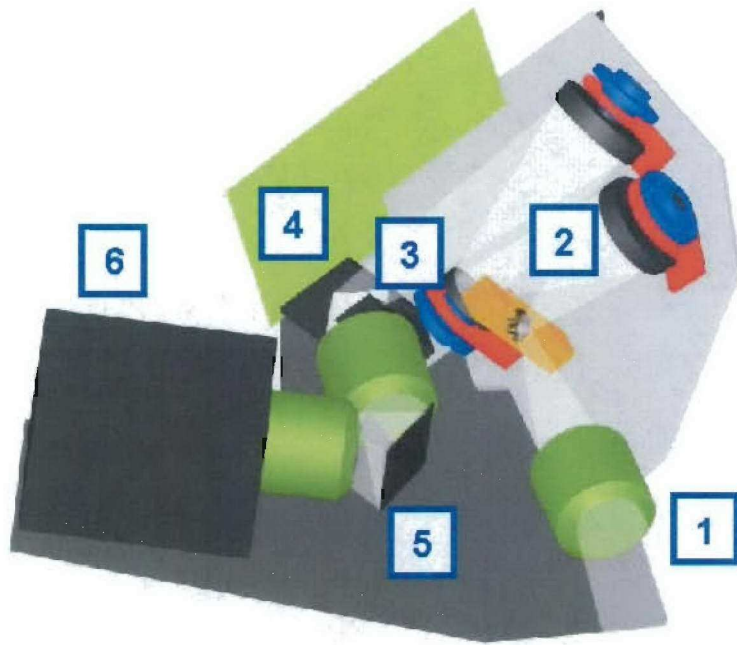


**Figure 9:** Solid model of NSTIS optical path and layout with labels which describe:

1. Camera lens front objective: a. Standard Canon manual FD mount b. Modular c. Transfers image of scene into system	2. All-reflective relay system: a. Transfers image from objective, conditioning it for DMD b. Custom PSS Optical design c. Flat to tilted image plane correction d. COTS spherical reflectors
3. TIR Prism: a. Transfers image onto and off of DMD b. Folds optical path c. Custom PSS design and coating for NIR wavelength region	4. DMD: a. Multiplexing component b. Modulates system resolution elements c. COTS TI MEMS mirror array d. PSS custom control electronics
5. Diffraction Grating: a. Dispersion component b. Spectrally spreads each “pixel” from the DMD	6. NIR Broadband camera: a. Indigo Phoenix NIR camera b. 900nm – 1700nm c. 640 x 512 pixels

Because of the tight placement of the DMD at the center of the optical path, previous control electronics would not fit within the system illustrated above. As a result, it was necessary to design and fabricate a new flexible circuit board, mated to our existing electronics, that allows for better positioning of the DMD and greater access to the component for optical purposes. These components are shown the next figure.

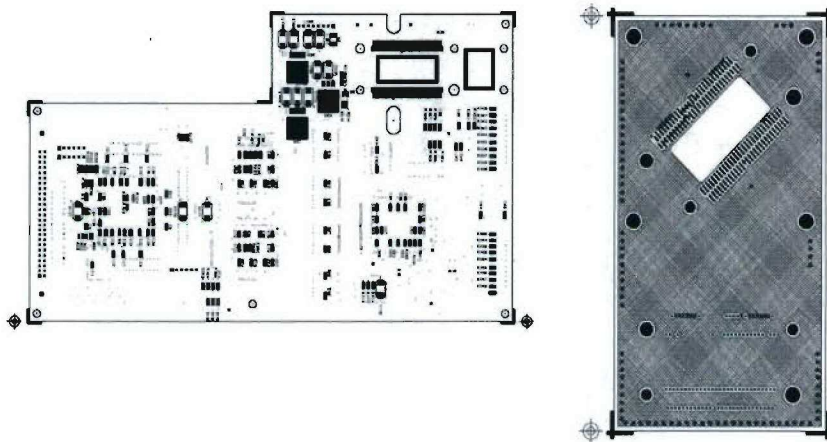


**Figure 10:** DMD driving electronics and flex circuit board (not to scale).

#### System Software:

NSTIS is operated with the real-time user interface application NstisAppR, a GUI that supports hyperspectral image preview, acquisition, review, and storage. It handles all communication and control between the PC, the DMD electronics, and the Indigo Phoenix™ camera. NstisAppR is primarily a data collection application with a few simple analysis tools included. More substantial post-collection data processing capabilities may be added in future versions.

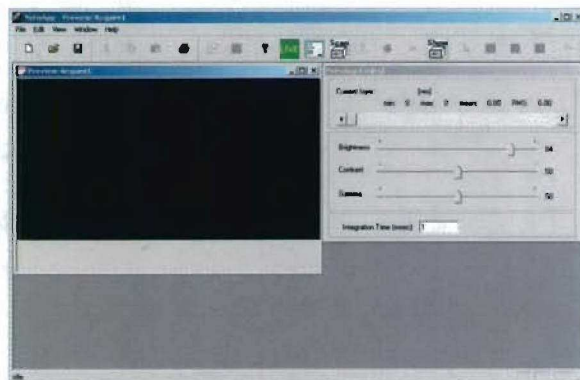


**Figure 11:** NSTISAppR start-up.

The exact type of acquisition as well as any post-acquisition processing is determined by settings in the parameter dialog as shown in the next figure.

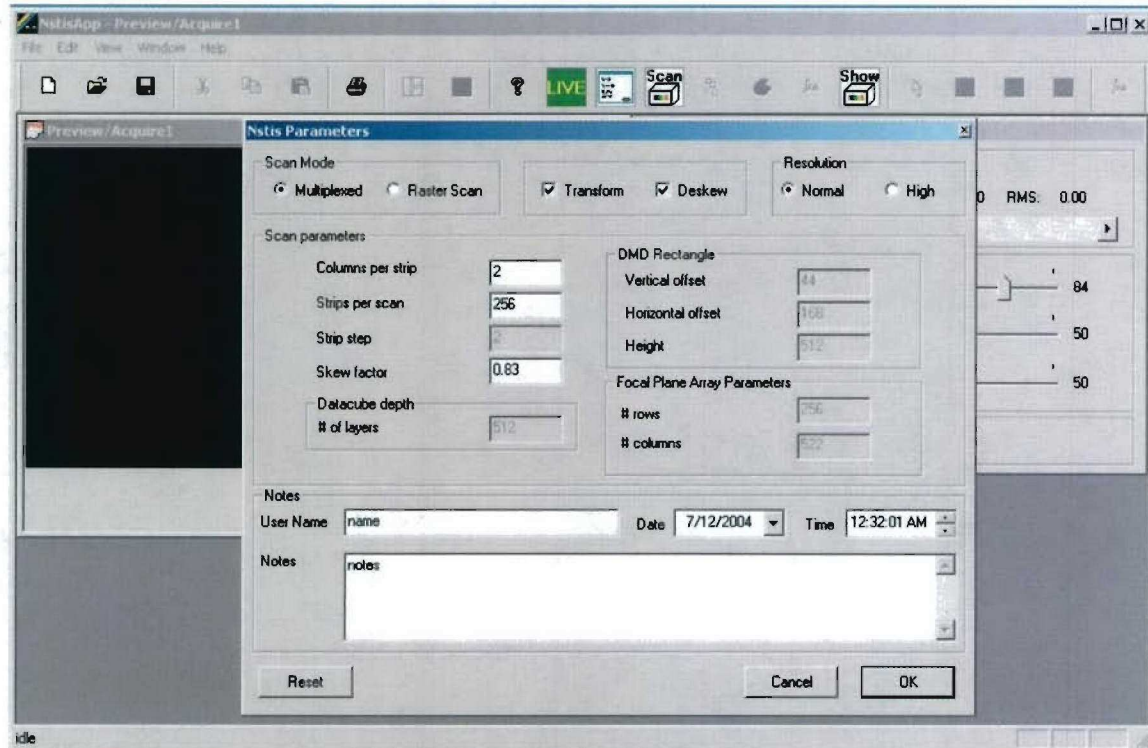


**Figure 12:** NstisAppR parameters.

NSTIS supports the two scan modes, “multiplexed” (Hadamard) and “raster”. In multiplexed scan mode, multiple overlapping spectra from various columns of the image are acquired per frame (multiplexed) and then mathematically transformed (de-multiplexed) to reconstruct the hyperspectral datacube. In raster scan mode, only the spectra corresponding to a single column of the image are acquired per frame. Multiplex mode enables data acquisition in lower light situations, while raster scan is appropriate when there is too much light for multiplexing.

NSTIS supports image acquisition at normal and high-resolution. In the optical configuration of NSTIS, each pixel of the Phoenix camera “sees” 4 pixels of the DLP. When normal resolution is selected, the 4 pixels are averaged. In high-resolution acquisition mode, the 4 pixels are used to sub-modulate the pixels of the camera, thus enhancing system resolution. When high-resolution mode is used, the result is a datacube that is 8 X larger (2 X in each dimension), enhancing datacube size from 256x256x266 to 512x512x532.

After acquiring a data cube NstisAppR can immediately perform two post-acquisition procedures: an inverse transform procedure when in multiplex mode and a deskew procedure. When the Deskew check box is checked, the acquired data will be deskewed. This means that the spatio-spectral direction of the system will be “unwound”, so that the datacube will be presented as 2 purely spatial dimensions, and 1 purely spectral dimension.

Acquired data cubes can be viewed, wavelength by wavelength, in an automated or user-controlled way via a slider control as shown in the next figure.

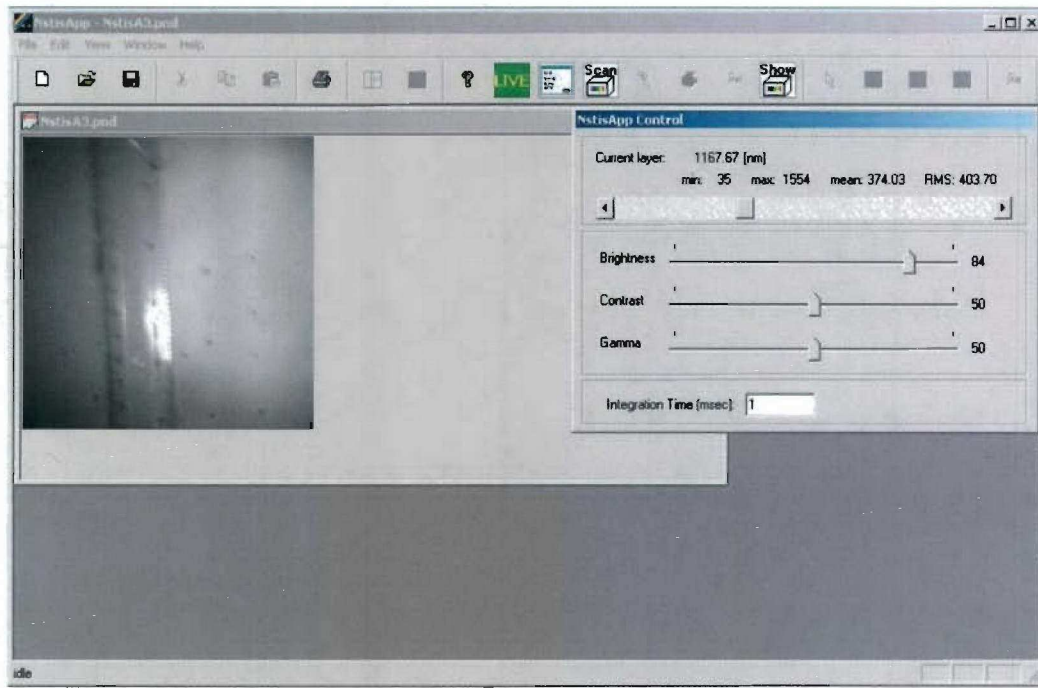


**Figure 13:** Reviewing an acquired cube.

Acquired data cubes can be saved into disk files and later reloaded into NstisAppR. Cubes can also be exported to file for further processing in Hyperspectral Explorer, HSE, optionally available with NSTIS, as well as in MATLAB™. Data can also be exported to a variety of other file formats as well as directly into the HSE application.

### Sample Data:

The following figures show hyperspectral images and sample spectra as acquired using the NSTIS system.

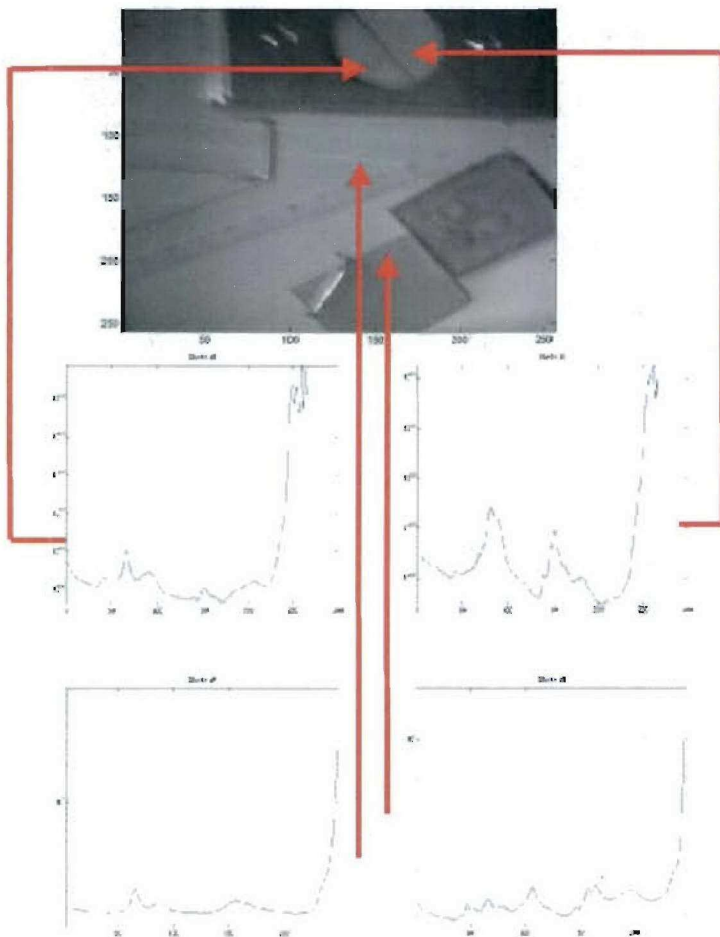


**Figure 14:** A scene consisting of a number of different plastics and other materials imaged with the system and displayed at one wavelength. Spectra of the various plastics in the scene, as acquired by the device, are shown below the image as indicated. Some analysis of this hyperspectral dataset using HSE is demonstrated in the next figure.

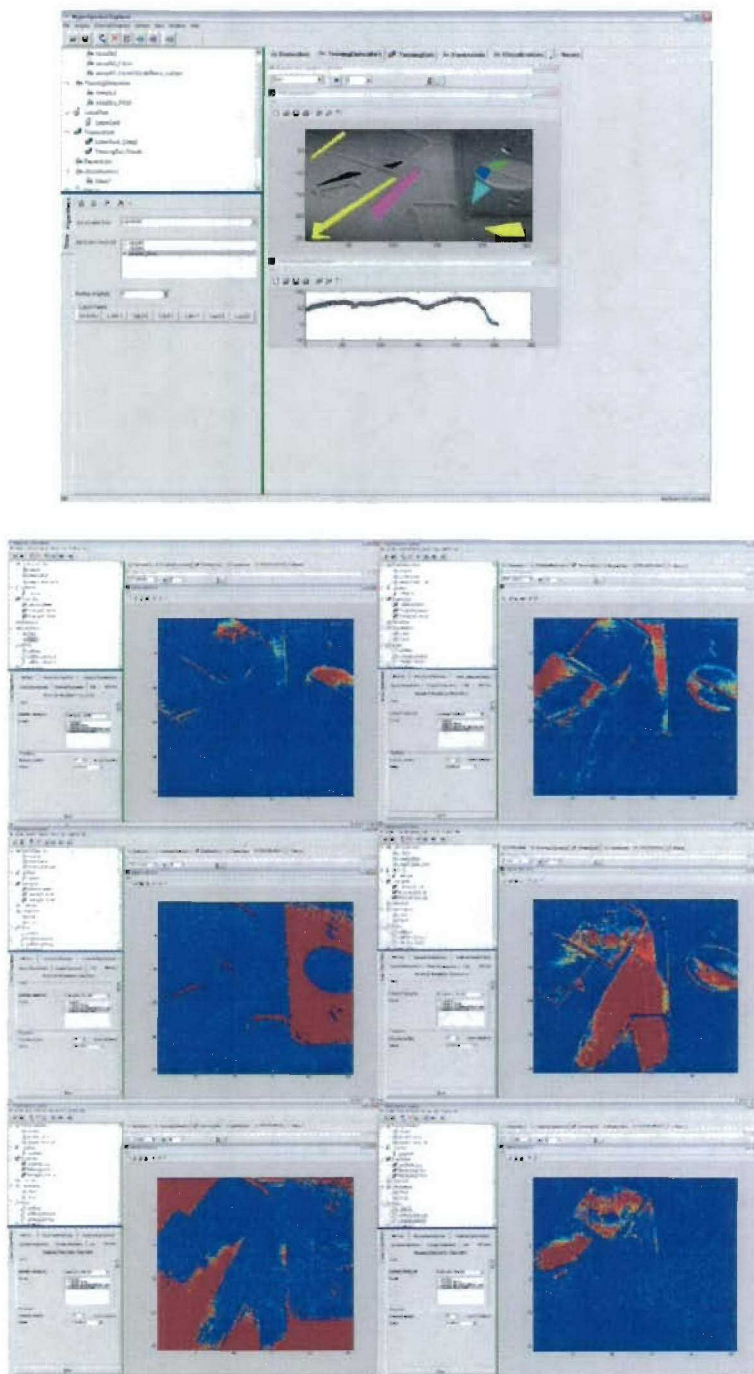


**Figure 15:** This figure shows screenshots of analysis performed on the hyperspectral dataset of the previous figure using the HyperSpectral Explorer platform (HSE). The top image shows the user-selected regions of the image designated as training sets. The subsequent screenshots each show the resulting factor analyses. Materials of different chemical compositions become differentiated.

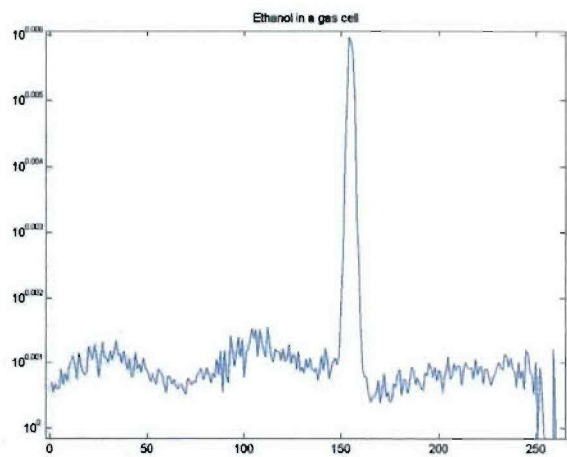


**Figure 16:** Spectrum of Ethanol measured by imaging a gas cell. Broadband image on left; extracted raw spectrum on right.

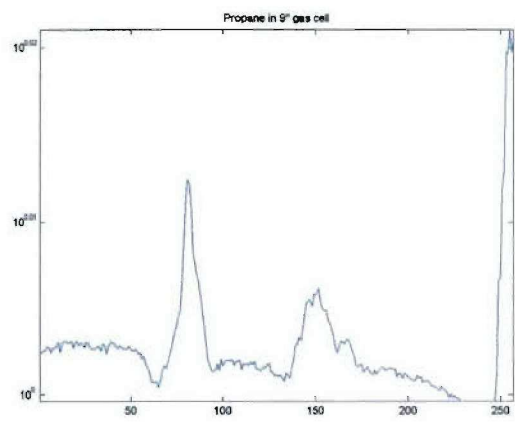
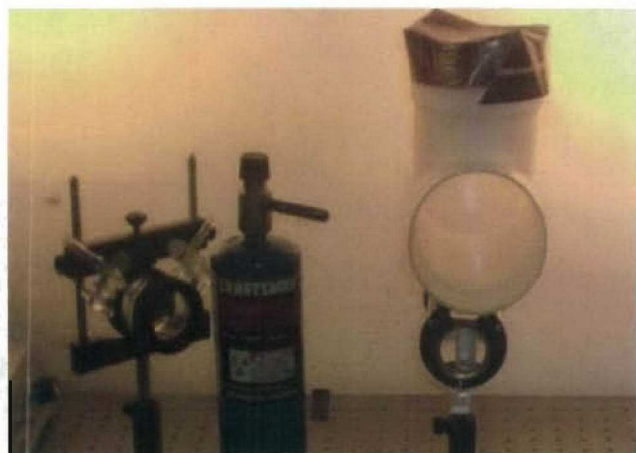


**Figure 17:** Spectrum of Propane measured by imaging a gas cell. Broadband image on left; extracted raw spectrum on right.

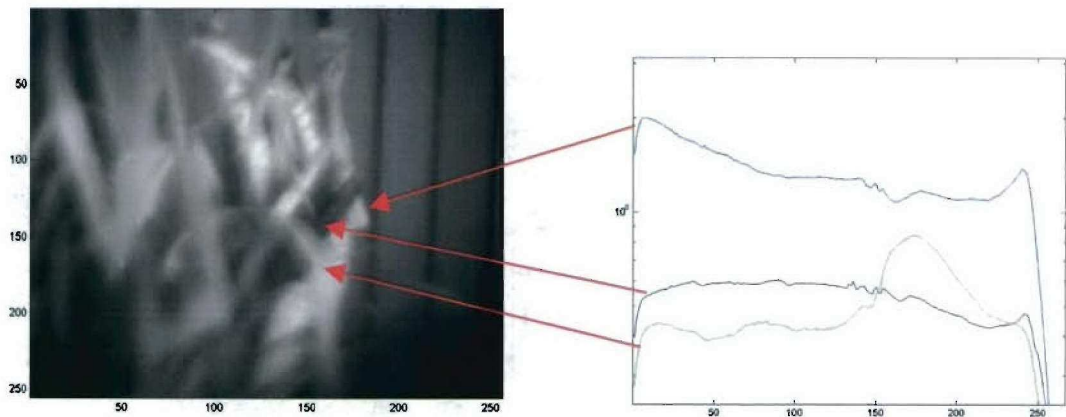


**Figure 18:** Spectrum of palms (real and artificial) in NIR hyperspectral image collected indoors.

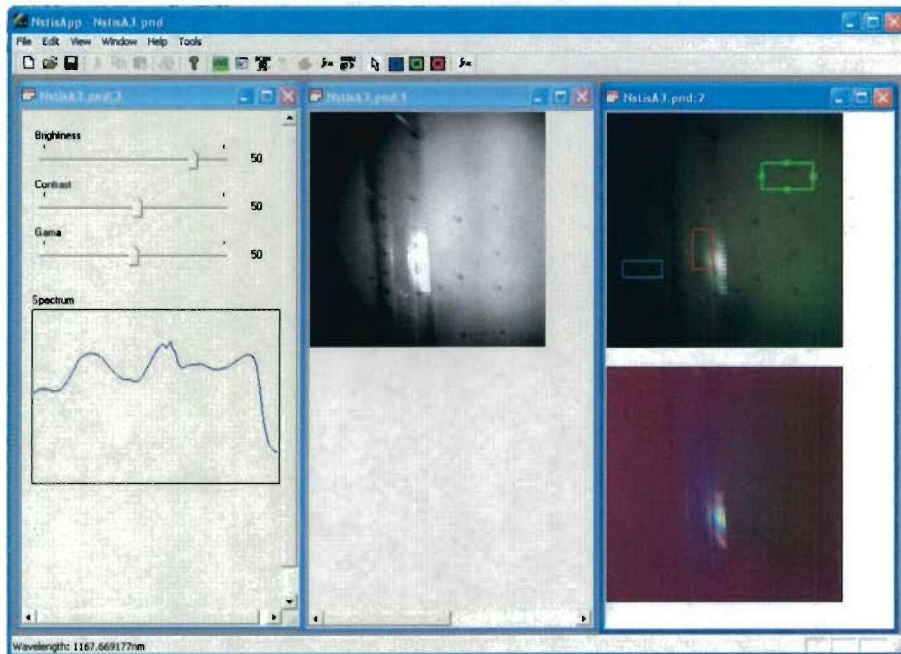


**Figure 19:** Screenshot of NstisAppR with acquired image of polystyrene ruler illustrating the basic analysis tools included; advanced processing on the data is to be done elsewhere with other software (e.g. HSE).

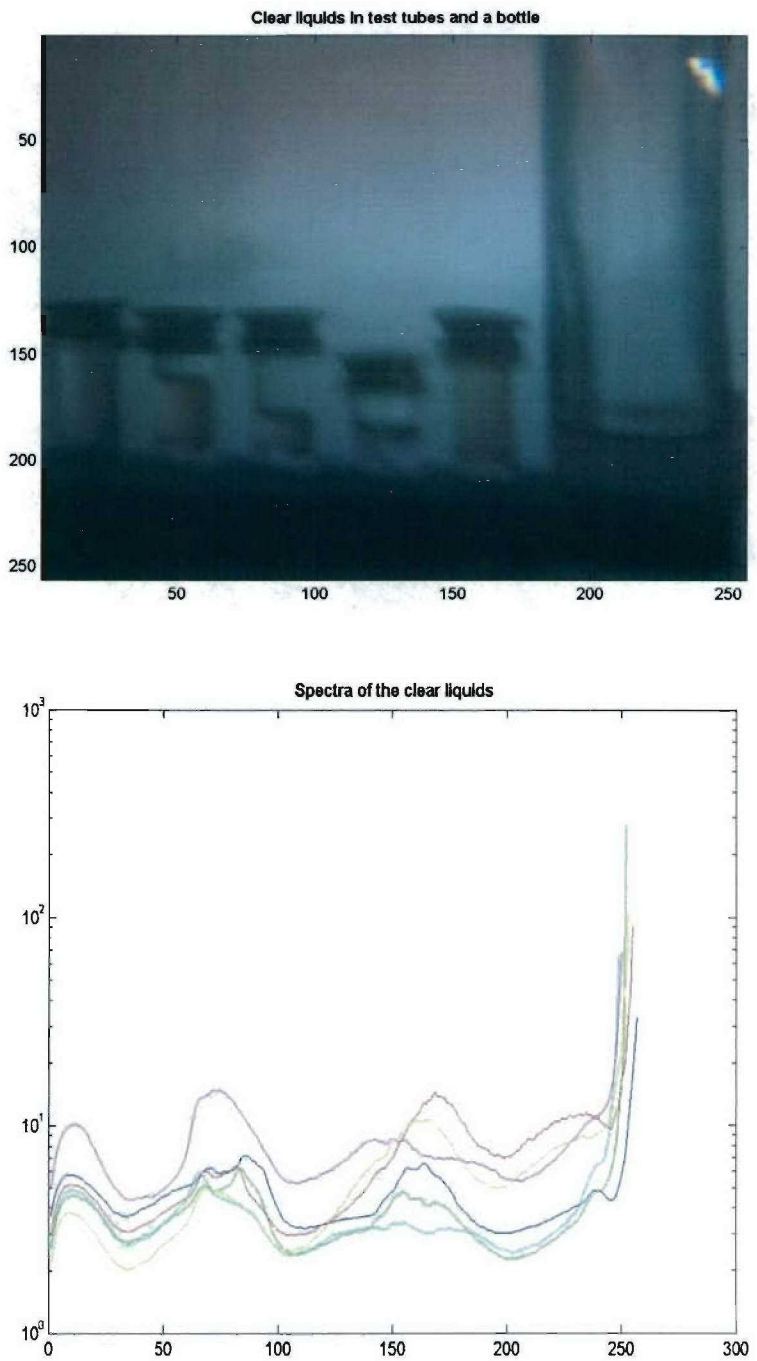


**Figure 20:** The top image is of a set of vials containing various transparent chemicals. It has been pseudo-colored to reflect the chemistry revealed by the underlying hyperspectral data. Whereas the chemicals are transparent and identical in appearance in visible light to the human eye, this shows them with different tints of color reflecting their different chemistries as measured in the NIR. The lower image shows the raw spectra measured by the camera from each of the chemicals in the various containers.

### **Second Build of Near Infrared System (8/2004 → Present)**

In the past year, Plain Sight successfully completed and tested a second NIR hyperspectral camera prototype (NSTIS2), incorporating design changes and improvements yielded from experience gained in building and fielding the first completed system. The following images show the system at various stages of assembly.



**Figure 21:** Main optical bench completed and displayed with uncoated optical mounting components.



**Figure 22:** Fully assembled system with covers removed to display internal optics and electronics.

**Figure 23:** NSTIS2

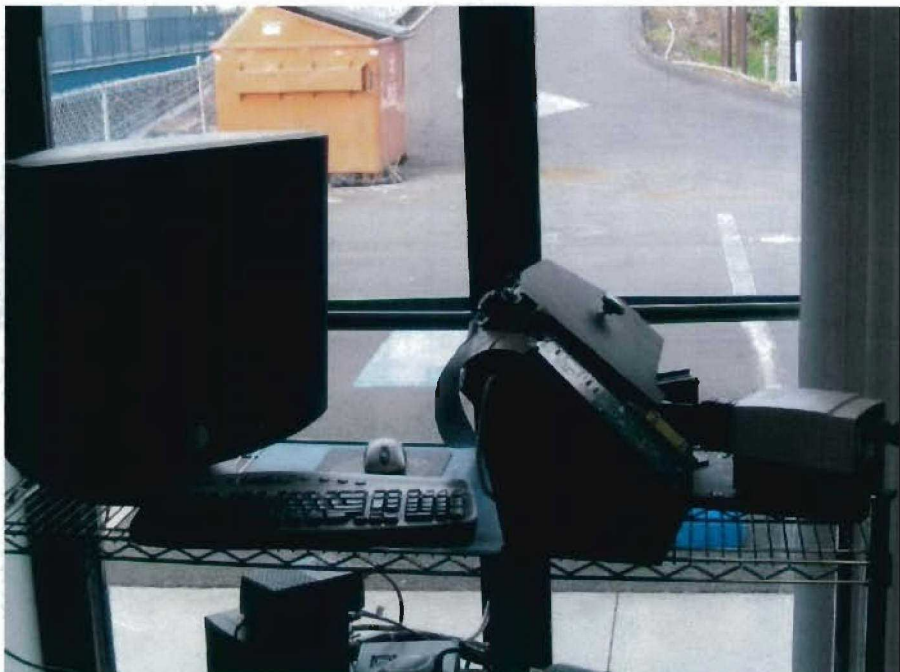


**Figure 23:** Completed NSTIS2 system deployed with PC in a mobile configuration. The system is shown imaging a natural scene through the window of building.

**Data Example from NSTIS2**

In the following example, a transparent panel of Lucite and portion of camouflage tarp were hidden in a natural scene. As illustrated by Figure 24, an image of the scene taken by a regular RGB digital camera, these objects were difficult to pick out with the naked eye.

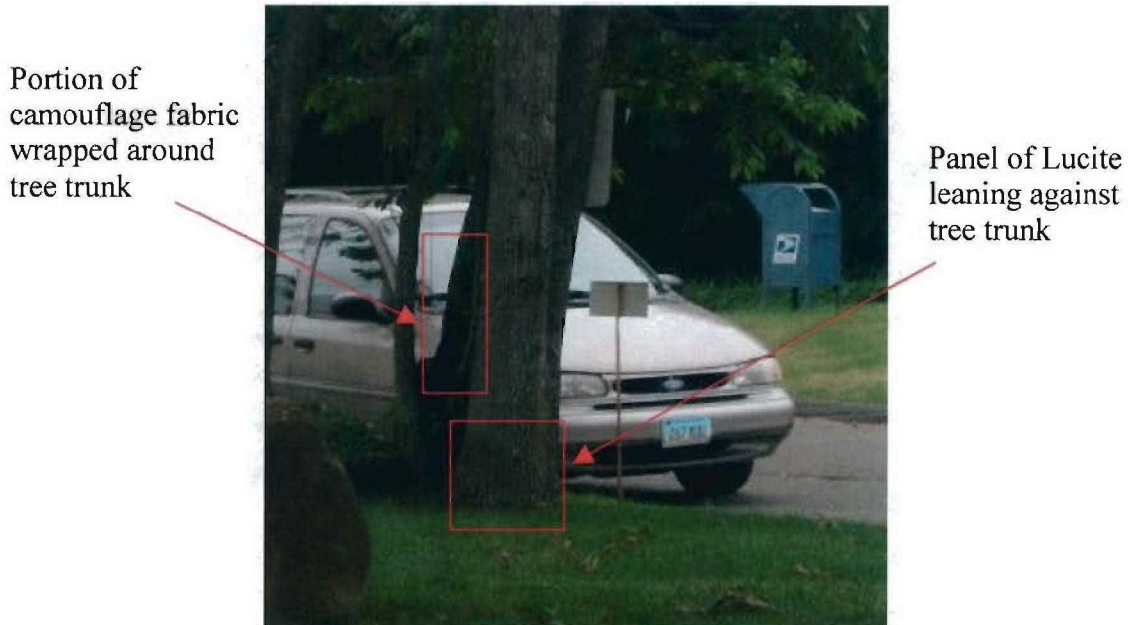


**Figure 24:** Natural scene imaged by conventional high resolution RGB digital camera with hidden items indicated.



**Figure 25:** Selected feature image from hyperspectral datacube of scene acquired by NSTIS2 system. Both the camouflage fabric and Lucite panel appear dark with respect to background and are no longer difficult to see.

## **China Lake Data Collection and Analysis – Demonstration of Chemical Sensing (9/2004 → Present)**

Work was performed under this contract in support of field studies and development described in this section in so far as it was related to hardware and design modifications. Other support and activity by Plain Sight Systems and other parties involved, was chiefly funded by other sources and contracts as well as Plain Sight cost-share. We include documentation of this activity as it was in part enabled by our work under this contract and also to illustrate the success of the NSTIS system in demonstrating the technology developed under this contract.

In September 2004, the NSTIS system was sent to the China Lake Naval facility where, in collaboration with NAVAIR and a group from Lockheed Martin's Missiles and Fire Control division, Plain Sight collected a significant amount of data of various targets of interest. This activity was also partially funded by other sources as well as Plain Sight cost-share. Prior to deployment, work was done hardening the mounts, modifying the base to mate to a specific tripod, improving ESD protection, and evaluating a series of imaging optics both custom and COTS.



**Figure 26:** NSTIS camera fielded at NAVAIR China Lake facility. The system was fielded in a mobile configuration with tripod and telescopic imaging lens. Majority of data was collected through an open window on the upper floor of a large building.



**Figure 27:** RGB digital camera image of view from vantage point of NSTIS camera location.

In the scene of Figure 27, we see a camouflaged truck that was almost a quarter mile distance from the location of the NSTIS camera. In front of the truck is a person next to whose feet were placed glass containers that were imaged filled with various chemicals. The glass and chemicals were all transparent and not visible to the naked eye at that distance. The next image shows data acquired by NSTIS, from the same vantage point, with a telescopic lens focused on the region of interest.

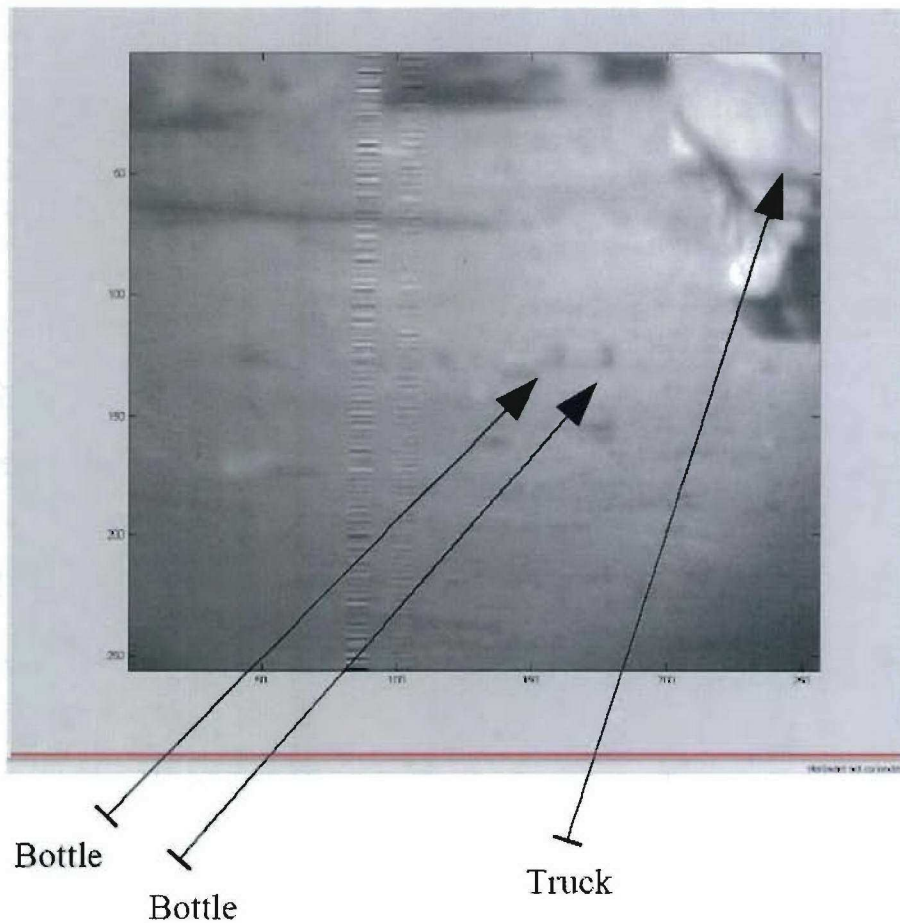


**Figure 28:** A selected narrow NIR wavelength band image of datacube acquired by NSTIS with telescopic lens. Labels indicate the location of the two chemical containers and the back of the truck that was also shown in Figure 27.

As we see in Figure 28, the chemicals that were not visible to the naked eye now begin to become visible in a selected narrow NIR wavelength band in which they both absorb energy. The following figures illustrate further processing of the data and resulting spectral features that easily distinguish one gas from the other.

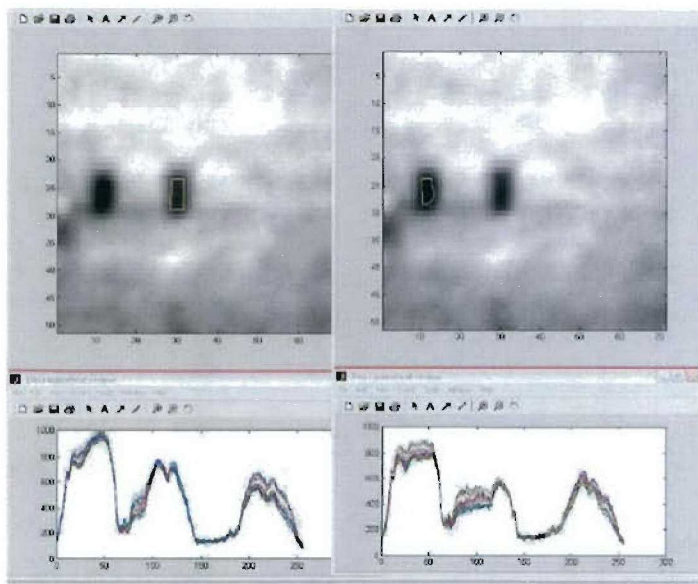


**Figure 29** : Sample spectra for each chemical extracted from the hyperspectral datacube.

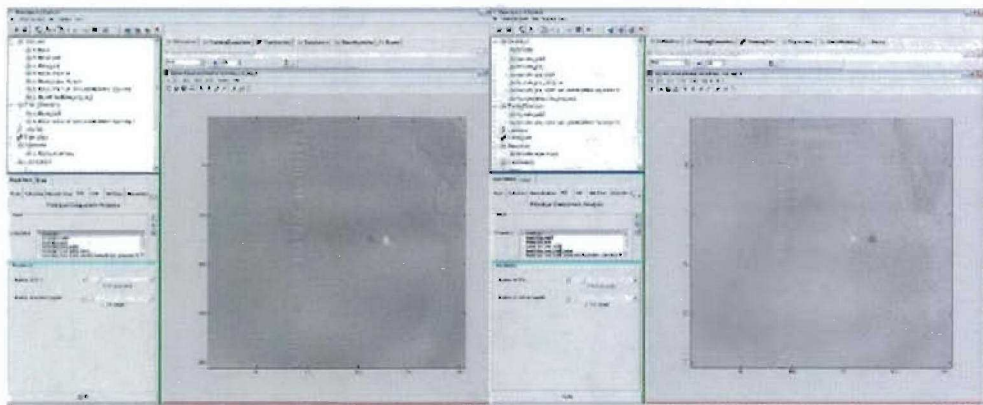


**Figure 30** : Sample analysis using Hyperspectral Explorer finds spectral features which locate and discriminate one chemical from the other.

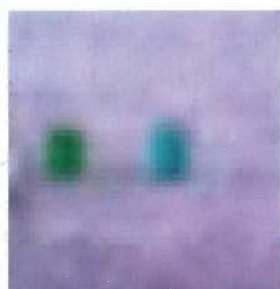


**Figure 31** : Using this analysis of spectral features, a pseudo-colored image of the region of interest is produced that both locates and discriminates the two chemicals.

## Lockheed Martin Data Collection and Analysis (4/2005 → Present)

Work was performed under this contract in support of field studies and development described in this section in so far as it was related to hardware and design modifications. Other support and activity by Plain Sight Systems and other parties involved, was chiefly funded by other sources and contracts as well as Plain Sight cost-share. We include documentation of this activity as it was in part enabled by our work under this contract and also to illustrate the success of the NSTIS system in demonstrating the technology developed under this contract.

The main data for the study was collected at the Lockheed Martin Orlando facility in April 2005. From a collection tower, a set of datacubes was collected for a background scene as well as for a target (a vehicle) moving right to left at various time steps (see Figures 32 and 33). The data was used to demonstrate detection and localization capabilities of an integrated sensing and processing suite consisting of dynamically programmable DMA sensor (NSTIS) and adaptive algorithms.

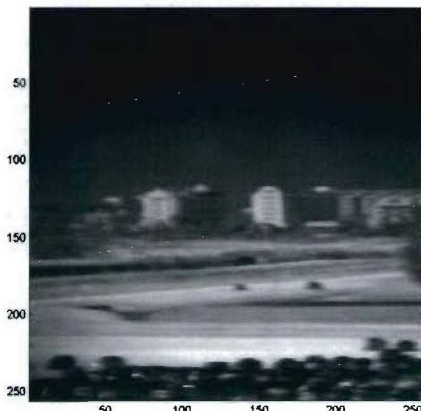


**Figure 32:** NIR broadband image of sample datacube acquired by NSTIS of parking lot, roads, and buildings as viewed from vantage point at Lockheed Martin Orlando facility.



**Figure 33:** Image from localized datacube acquired by NSTIS with target box indicated in red that was used to train algorithm.

Some results of this activity were described the in the article: “An Application of Integrated Sensing and Processing Decision Trees for Target Detection and Localization on Digital Mirror Array Imagery” by Priebe, Marchette, Park, and Muise, submitted for publication in Applied Optics. A draft of this article is included as an appendix to this document to illustrate a demonstration of integrated sensing and processing using NSTIS in the field.

## **Future Plans**

Plain Sight is enthusiastic to continue to pursue and develop this technology and the possible opportunity to insert it into defense applications as well as some in the commercial sector. Together with a group from Lockheed Martin's Missiles and Fire Control division, we plan to continue a series of tests and demonstrations with various possible customers from defense agencies. It is already the case that the NSTIS system is to be scheduled for demonstration at another military facility (Marine Battle Labs) during 2006.

Also currently under investigation are possible applications to the environmental and petrochemical industries that Plain Sight has been developing through work outside the scope of this contract.

## Concepts Demonstrated

### Scanning without macro-motion

Prior art passive hyperspectral imaging systems have all required macro-moving parts to achieve hyperspectral imaging of a two dimensional scene: either physical scanning of the camera, the object of interest, or some macro-mechanical part such as a rotating prism or a scanning mirror were required. By scanning through a sequence of slits or encodements on the DMD, the present system can image a full hyperspectral datacube without any such motion (only MEMS array elements move, by about 4 microns maximum displacement at the corners of each element). Of course, hyperspectral imaging can also be achieved with tunable filters that effectively raster scan in spectral domain. Although such systems are simple, they are inefficient and do not have multiplexing capabilities.

### Multiplex advantage

The following sequence of images demonstrates the multiplex advantage associated with Hadamard encoded scans versus raster scans. The experimental setup consisted of the third prototype system described above with a Sigma Lens (50mm, f2.8, Macro Lens, Nikon mount), focused for roughly one to one imaging on a sample of didymium, scotch-taped to a sheet of 20# bond copy paper, with a blotch of ordinary ballpoint pen ink on the scotch-tape. The scene was illuminated from behind with a LabSphere™ integrating sphere with an IHLS-100-125 125W Halogen light bulb. The resulting amount of light was somewhere between that present in a scene illuminated by bright sunlight and that of one illuminated by typical indoor office lighting.

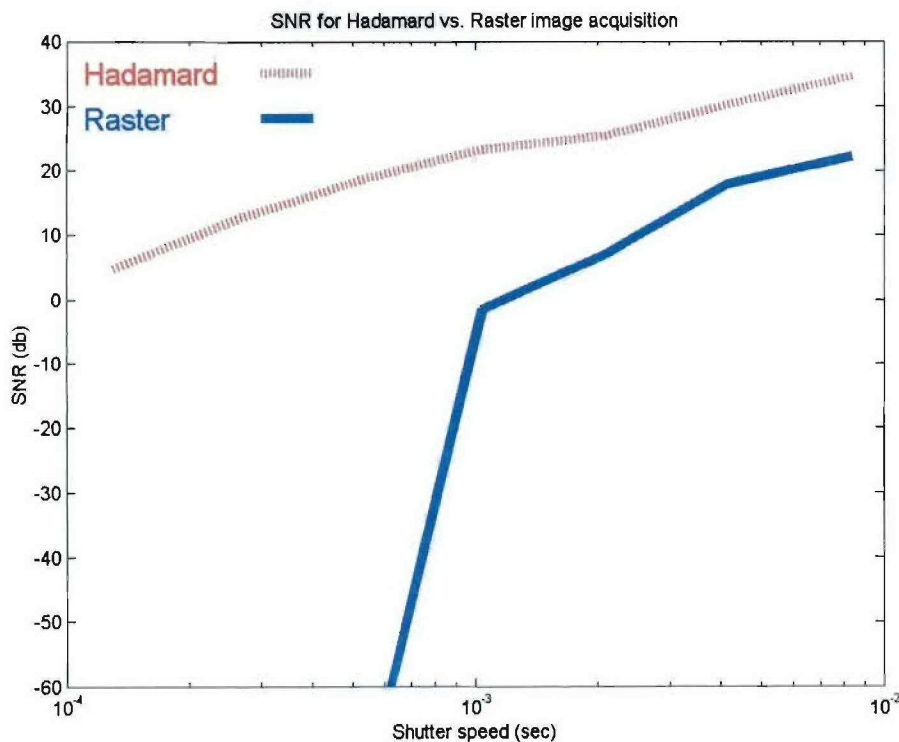
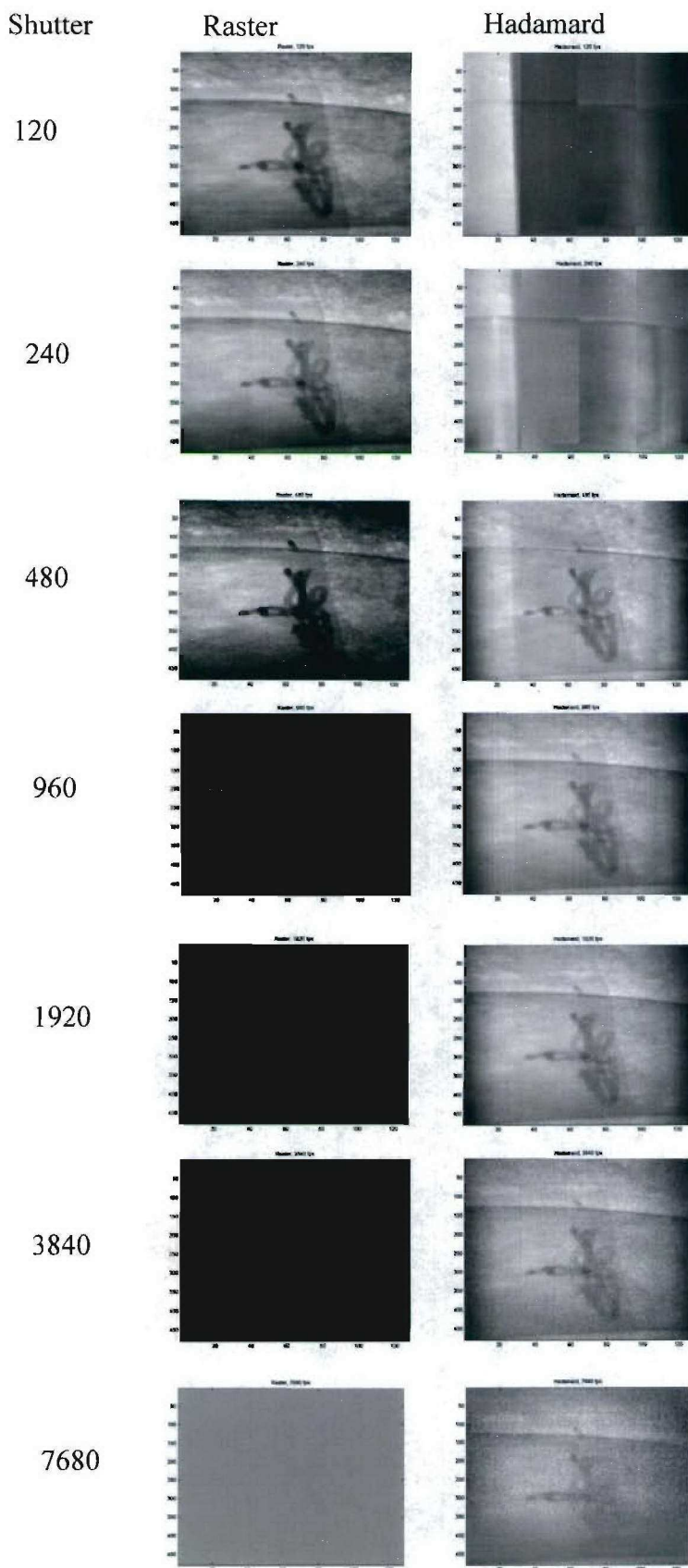


**Figure 34:** SNR graph demonstrating multiplex advantage (3<sup>rd</sup> generation system).



Note: In Hadamard mode the camera was blooming until the shutter speed was lowered to about 1/1000<sup>th</sup> sec.

**Figure35:** Image sequence demonstrating multiplex advantage.

## Adaptive multiplex advantage

The preceding section demonstrated that multiplexing is an advantage in low light situations, and actually causes artifacts when there is plenty of light. Hence, depending on the amount of light present in a scene, it might not always be optimal to multiplex. Moreover, one can raster scan through a tiling of sub-regions in a scene, and multiplex within each sub-region, in an adaptive fashion. In this way, the device can be used to automatically multiplex at an optimal level (provided that lighting conditions do not change much over the time scale of a pair of scans). The following graph demonstrates the added advantage achieved by multiplexing at the appropriate scale.

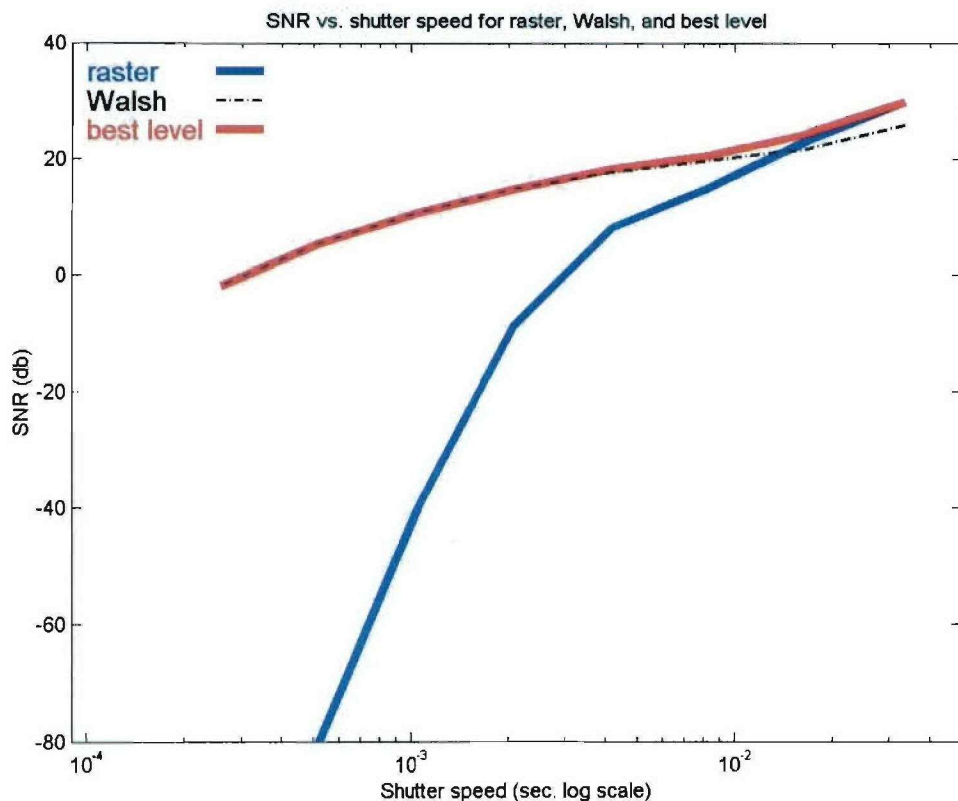


**Figure 36:** SNR graph demonstrating adaptive multiplex advantage (3<sup>rd</sup> generation device).

## Feasibility of video-rate passive hyperspectral image data acquisition

The data above demonstrate that in appropriate lighting conditions, our device can collect raw video frames at about 9000fps. Since a typical datacube is 640x480x128, this amounts to collection of about 70 full hyperspectral frames per second. Modern DSPs are roughly capable of providing relevant processing of the resulting ~2.5Gigabytes/sec of data, if highly optimized, and offline preprocessing is allowed. Compression and adaptive measurement schemes being investigated under this project could enable more sophisticated processed acquisitions with less

processing power. While the data shown above reflects electronic shutter speed and not actual frame rate, experiments performed with a RedLake™ high-speed CMOS imaging system demonstrated the feasibility of actual high-speed image acquisition at several thousand raw frames per second with our current system.

## **Feasibility of natural Light Hyperspectral Imaging with Multiplex Advantage**

In 2003, Plain Sight demonstrated the ability of the system to collect hyperspectral datacubes in ordinary room light, and in sunlight. As mentioned above, we were able to collect quality datacubes from ordinary objects using ordinary indoor commercial overhead fluorescent lighting, as well as a number of datacubes with the device pointed out the window of our facility, spectrally imaging automobiles, trees and grass in the area. The system's electronic control and shutter allows it to be easily tunable to different conditions. The device was sensitive enough that we were able to image outdoors all the way at F/22. We were able to collect data until about 7:45pm Eastern Time in summer, when the sunlight is fading and dusk is settling in.

### System Performance Characterization

**Spatial resolution** – This is determined by the swappable fore-optics. The system is typically used in a one to one imaging mode, so that individual pixel spatial resolution is nominally 17 microns, and line pair resolutions at about twice this dimension have been typical with the current prototype. When mounted on a microscope, the total system spatial resolution scales accordingly.

### **Spectral range and resolution**

Nominal spectral resolution is on the order of 2nm, depending on system alignment, and could be made higher or lower with a different choice of grating. The spectral range is roughly 400nm – 1100nm or 900nm – 1700nm, with approximately 350 pixels of data per cube, in the spectral direction. Typical spectral resolution, FWHM, is about 15nm.

### **Data collection speed**

The system has collected reasonable data at shutter speeds as fast as 1/10000 sec. At the moment, acquisition and processing electronics are the bottleneck to faster data acquisition, in spite of the fact that sub-optimal opto-mechanical components are employed in the current system. The existing prototype collects 20 fps in its fastest mode, for a rate of one 640X480X128 datacube every 6.4 sec. With a fully integrated and engineered solution, the system could collect data at video rates, as described above.

### **Light power at image sensor**

In one experiment, the light power at an image sensor was measured to be:

Background: .011  $\mu\text{W}/\text{cm}^2$

Raster scan: .124  $\mu\text{W}/\text{cm}^2$

Hadamard Scan (128 elements): 2.56  $\mu\text{W}/\text{cm}^2$

## Aberrations and other problems and lessons

### **Sensor non-linearity and multiplexing artifacts**

As long as the system was not blooming the multiplexing helped to achieve low light level imaging. When the sensor bloomed, artifacts were present. The first few multiplexed images in Figure 23 demonstrate this effect. The present system is capable of adapting to varying light conditions as described previously.

### **System misalignment and multiplex artifacts**

As a prototype static hyperspectral imaging system, device performance and design goals were achieved and even surpassed. However the system is prone to alignment and stability issues that could be solved by an opto-mechanical engineering effort and funding to accomplish this.

Multiplexed artifacts are predicted and observed in association with a data skew resulting from these alignment and optical design issues. It is not currently possible to have the system both horizontally and vertically aligned: there is a trapezoidal image plane. Our multiplex algorithms assume a rectangular acquisition. Because multiplexed data are quantized by the A/D converter of the image acquisition, this results in an artifact with structure related to the multiplexing scheme used. Walsh multiplexing results in a multi-scale grid artifact, and pseudo-random Hadamard codes can be used to mitigate these effects. These issues are present, but are minor under most lighting conditions (i.e. measurable only in the bottom bit of the A/D). The effect can be mitigated by pre-computation that would dictate a modified mirror driving setup that compensates for the geometric aberrations.

### **Vignetting**

Vignetting is severe in this system and in some instances possibly in excess of 50% due to some of the cots optical elements employed in the imaging spectrograph portion of the camera system. The selection of better optics would resolve this issue.

## Spectral Target and Anomaly Detection

The following two examples demonstrate target and anomaly detection enabled by the hyperspectral imaging system.

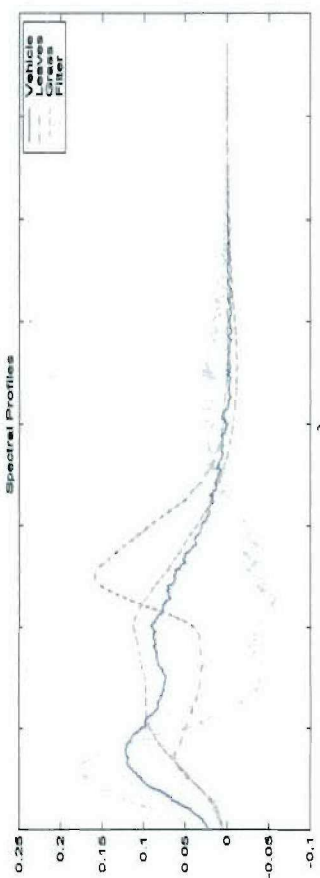


**Figure 37:** Camouflage detection simulation images.

In the figure above, the top left image was taken with an ordinary digital color camera, the image below shows the visible wavelength portion of the broadband scene, as seen by our camera, upper-right image shows the result of orthogonal processing of the target vs. the background in gray level, and the lower-right image shows an RGB rendering of spectral energies of the vehicle, leaves, grass and orthogonalized vehicle detection filter.

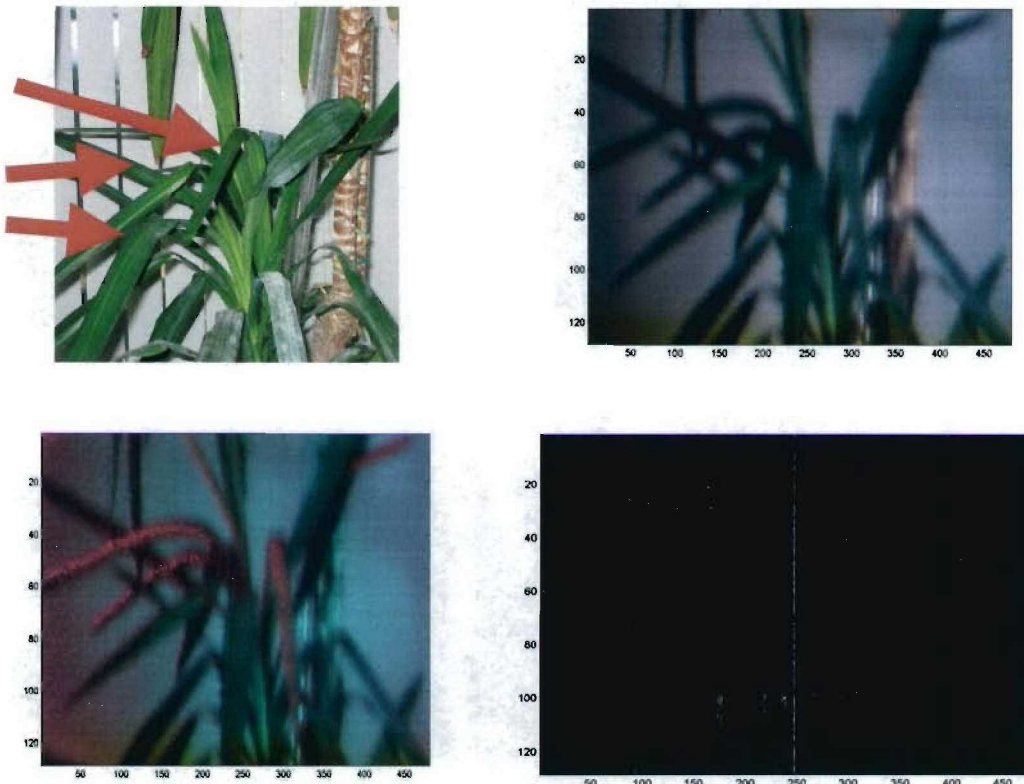


**Figure 38:** Fake vegetation is discovered easily through the standoff coded aperture imager, Bottom right; a conventional spectrograph image under same light integration setting.

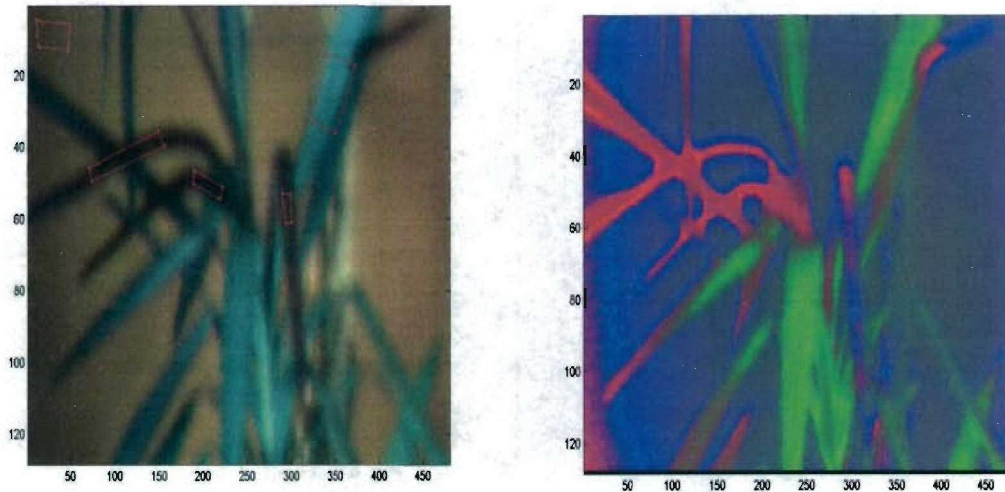


**Figure 39:** Camouflage detection simulation images. Selected filter designs for discrimination. The left image represents a combination of bands converted to RGB. The right image uses best discrimination spectral filters converted to RGB

## OPTICAL ISSUES

**ForeOptics:** The DMD is placed at the focal plane of a COTS Nikon optical system and exhibits excellent imaging properties and has a vast array of COTS lensing options. However, exact placement of the DMD at the focal plane has not been realized with the GEN1 prototype and TIR prism. We expect improved spatial resolution with subsequent generations. We have the advantage of selecting from the array of Nikon imaging optics as our applications are identified in more detail. The latest NSTIS system with Canon FD foreoptics has already greatly improved upon this.

**TIR prism:** The COTS total internal reflection (TIR) prism allows a more compact optical path and was engineered for a commercially available projector system. There are some stray light and dispersion issues relating to the TIR prism geometry that may reduce effectiveness for some low light applications.

We have found a multiple-bounce reflection image that manifests itself as an intensity modulated spatio-spectral image when the prism and grating are a particular coincident optical configuration. Testing and examination of this phenomenon can be accounted for and reduced or eliminated by rotating the relative scanning/dispersion dimension by 90 degrees to the TIR prism.

Additional improvements can be made by optical engineering efforts to produce a TIR prism assembly that is adapted to this application that will allow

- Lower F# operation/improved throughput
- Improved spectral resolution
- Reduced stray light
- Improved optical geometry
- More compact designs

**Imaging Optics – Spectrograph:** To keep costs to a minimum we have employed inexpensive COTS imaging optics in our spectrograph optics. This resulted in a sacrifice in F# and FOV that did not include the entire DMD object plane. Improving the selection of imaging optics in the spectrograph portion of the system will improve performance dramatically.

- Reduced vignetting
- Increase throughput (F# reduction to match NIKON-DMD optics)
- Improved spatial resolution
- Improved spectral resolution (Reduced chromatic aberrations in the NIR)
- Improved spectral response (VIS-NIR broadband AR coatings)

**Sensor:** The sensor employed for our first proof of concept device was based on a standard video camera, low performance and not of scientific quality, and did not match DMD pixels or format. The latest NSTIS system improves greatly upon this, employing a high quality sensor chosen to mate appropriately with the designed surrounding optics.

## **1. Appendix: Related publication demonstrating Integrated Sensor Processing (ISP) work done with NSTIS system.**

Priebe et al., “An Application of Integrated Sensing and Processing Decision Trees for Target Detection and Localization on Digital Mirror Array Imagery”, submitted for publication in Applied Optics, Draft dated July 18, 2005.

*Applied Optics*

# An Application of Integrated Sensing and Processing Decision Trees for Target Detection and Localization on Digital Mirror Array Imagery

Carey E. Priebe<sup>†</sup>, David J. Marchette<sup>††</sup>, Youngser Park<sup>†</sup>, and Robert R. Muise<sup>†††</sup>

<sup>†</sup>*Johns Hopkins University, Baltimore, MD*

<sup>††</sup>*NSWC B10, Dahlgren, VA*

<sup>†††</sup>*Lockheed Martin, Orlando, FL*

*Corresponding author: C.E. Priebe, cep@jhu.edu*

Draft dated July 18, 2005

We demonstrate the applicability of the Integrated Sensing and Processing Decision Trees (ISPDTs) methodology to a set of digital mirror array (DMA) hyperspectral imagery. In particular, we demonstrate that ISPDTs can be used to detect and localize targets using just a few DMA Hadamard frames, so that an entire hyperspectral data cube need not be collected in order to successfully perform the given task. This suggests that such an integrated sensing/processing suite may be appropriate for extremely time-sensitive pattern recognition applications.

© 2005 Optical Society of America

*OCIS codes:* 100.2960, 100.5010.

## 1. Introduction

We demonstrate the applicability of the Integrated Sensing and Processing Decision Trees<sup>1</sup> (ISPDTs) iterative denoising methodology to a set of digital mirror array<sup>2</sup> (DMA) imagery.

The sensor sequentially collects 256 Hadamard frames in order to produce a hyperspectral data cube that measures  $256 \times 256$  pixels spatially and consists of 266 spectral bands. However, the sensor is (dynamically) programmable; given a pattern recognition task of interest (detection/localization/classification) it is desirable to learn a sequence of just a few

Hadamard frames that will accomplish the task sans the requirement to collect (and process) the entire data cube.

We demonstrate the construction, on one training hyperspectral data cube, of an iterative denoising tree that allows for detection and localization of a target using just two Hadamard frames; the entire hyperspectral data cube need not be collected in order to successfully perform the task.

This proof-of-concept result suggests that an integrated sensing/processing suite consisting of a dynamically programmable DMA sensor and ISPDT processing may be appropriate for extremely time-sensitive pattern recognition applications.

## 2. Sensor & Data

### 2.A. *Sensor*

The sensor under consideration is a prototype system developed by PlainSight Systems which incorporates a DMA device in order to realize a Hadamard multiplexed imaging system.

The known signal-to-noise (SNR) advantage in Hadamard spectroscopy<sup>3</sup> extended to imaging systems<sup>4,5</sup> allows for the collection of a hyperspectral cube of data with more efficient light collection than standard “pushbroom” hyperspectral imagers.

The PlainSight sensor is a spatial light modulator-based multiplexing hyperspectral imaging camera, operable in the near-infrared spectral range of about 900 nm - 1700 nm. The system uses a DMA commercially available from Texas Instruments for projector display applications. The DMA contains 848 columns and 600 rows of mirrors and measures 10.2 mm × 13.6 mm.

When the scene is illuminated on the DMA device, a standard raster scan could be implemented by turning the first column of mirrors ON, sending this column to a diffraction grating which results in a spectral representation of the first spatial column of the scene being illuminated on the detector array.

If one opens multiple slits in the DMA array, the detector array will be presented with the superposition of many columns of spectra. This system would have the advantage of optimal SNR when the pattern of the open slits form a Hadamard pattern.<sup>3</sup> Each individual frame at the detector array has less physical meaning than in the pushbroom method, but when all the patterns of the Hadamard sequence have been recorded, the full hyperspectral datacube is recoverable.

The PlainSight sensor implements the process wherein the detector array is a standard Indigo Phoenix large-area InGaAs camera operating in the near-infrared wavelengths.

During standard operation of the system, the sensor collects 512 frames. Each frame is 522 × 256 pixels and represents spectra vs spatial row. The 512 frames that are collected are based upon 256 Walsh (0s and 1s) patterns. Since the theory of optimal SNR is based

upon Hadamard (1s and -1s) patterns, one needs to collect two Walsh patterns to generate a single Hadamard pattern. Thus, the 512 collected frames represent the required Walsh patterns to form a full set of 256 Hadamard patterns. Since each column in the DMA array will hit the diffraction grating at a different location, the spectra will hit the detector array at a different location per column. We describe this as a “skewness” in spectra and results in the 522 pixels in the spectral dimension in order to represent the 266 actual spectral bins. Of course, this spatial/spectral mixing and skewness is invertible once all 256 Hadamard patterns have been collected. The resultant hyperspectral scene is dimension  $256 \times 256$  with 266 spectral bands from  $900\text{ nm}$  to  $1700\text{ nm}$ .

The sensor has the capability to utilize adaptive Hadamard frame collection schemes, as follows. The sensor is dynamically programmable, in that it can be tasked to render any Walsh pattern, at any scale, and at any location on the DMA. For example, standard operation of the sensor renders 512 Walsh patterns from the lowest spatial frequency to the highest, at a resolution of 256 mirrors. In adaptive operation of the sensor, any one of these patterns can be rendered on the DMA, an image frame is captured, some data processing can occur leading to a decision regarding the next frame, and then any of the other patterns can be rendered. This sensor capability allows one to task the DMA to render patterns that have been algorithmically calculated to be “optimal” given the data that was previously observed. (This adaptive sensor operation implies that the actual hyperspectral cube may no longer be recoverable from the frames collected, as one requires the full 256 Hadamard patterns be collected in order to invert the spatial/spectral mixing caused by the multiplexing. If the desired processing does not require the inverse operation be available, then it is more efficient to not collect all the data. We collect only what the algorithm needs to perform its function.) Thus, the dynamic programmability of the sensor allows one the flexibility to sense only that data which is required for the image processing task at hand.

Our task for integrating sensing and processing is to develop a scheme to collect these Hadamard frames one at a time, and make inferences about the current hyperspectral scene — and about the next Hadamard frame to be collected — as the frames are being sensed. Application may involve target detection/localization/classification as well as object tracking.

### *2.B. Data*

Data were collected at Lockheed Martin Orlando in April 2005. From a collection tower, a full set of 256 Hadamard frames was collected for a background scene ( $I_0$ ) as well as for a target (a vehicle) moving right to left at four time steps ( $I_t$ ,  $t = 1, 2, 3, 4$ ). Figure 1 depicts one Hadamard frame at time  $t = 2$ .

This collection of five hyperspectral scenes is used to demonstrate detection and local-

ization capabilities of an integrated sensing/processing suite consisting of a dynamically programmable DMA sensor and ISPDT processing.

### 3. Methodology

We apply the ISPDT iterative denoising methodology to the hyperspectral vehicle imagery,  $I_t$ ,  $t = 0, 1, 2, 3, 4$ , described above.

We use the hyperspectral data cube collected at time  $t = 2$ ,  $I_2$ , as our training data; Figure 1 depicts Hadamard frame 110 at time  $t = 2$ . We focus on  $64 \times 210$  image swaths, so as to obviate issues of sensor skewness and edge effects; Figure 2 depicts the swath for Hadamard frame 110 of the training data  $I_2$ , with the region delineated by the small box representing the training information regarding the target of interest. (No additional information regarding vehicle/non-vehicle pixels within the target box is utilized.)

Training proceeds as follows; see Figure 3.

#### 3.A. Step 1

No single Hadamard frame provides adequate performance in segregating target from non-target pixels, and so Hadamard frame 110 is selected for use at the root by virtue of its performance in providing the most clustering clarity — a new Hadamard frame at each node is determined based on the best separation between the target box and the non-target pixels by using the adjusted Rand index criterion.<sup>6,7</sup> Model based clustering<sup>8</sup> is employed, in which a Bayesian Information Criterion (BIC) is used to determine the complexity and type of a Gaussian mixture fit to the data. The clusters are then defined in terms of the posterior likelihoods of the individual components. The Hadamard frame 110 pixels (gray scale intensity) cluster into three clusters; the spatial location of the pixels for these three clusters are represented by blue, green and yellow in the root node of the tree depicted in Figure 3.

#### 3.B. Step 2

In building an ISPDT, after clustering at a node, each cluster is processed in a branch of the tree. This subsequent processing proceeds in an analogous fashion to that of the root: if the pattern recognition task at hand can be adequately addressed (for the data falling to that branch) then tree growth (along that branch) is halted. It is necessary, of course, to perform the search for the best Hadamard frame once again in each branch, conditionally upon the results of all previous clusterings.

In this application, the left-most (green) and right-most (yellow) clusters at the root of the ISPDT depicted in Figure 3 yield essentially pure non-target branches and no further tree growth is necessary in these branches, while the middle (blue) root cluster contains

many of the target pixels as well as a significant number of the non-target pixels. This middle cluster must be processed further. In this middle cluster, we find that Hadamard frame 151 provides clustering into two clusters; furthermore, one of these clusters (the left-most node at level three of the ISPDT depicted in Figure 3) contains a significant number of target pixels and no non-target pixels. Ergo, this leaf is labeled as the “target leaf”.

Notice that, as was mentioned above, no information regarding vehicle/non-vehicle pixels within the target box is utilized. Nevertheless, the “target leaf” (the left-most node at level three of the ISPDT depicted in Figure 3) successfully — and *unsupervisedly*, with respect to the pixels within the target box — makes this distinction.

The clustering at each level of the ISPDT can be used to produce a partition of the input space. Thus the ISPDT described above and depicted in Figure 3 can be presented as

$$g(x) = I\{x \in C_{1,2} \wedge x \in C_{2,1}\} \quad (1)$$

where  $C_{i,j}$  represents the  $j^{th}$  partition cell at level  $i$  of the tree and  $g$  is a classifier for pixel  $x$ .

Note that while the entire hyperspectral data cube was required for the training data, Equation 1 allows processing for detection/localization/classification with the collection of just two Hadamard frames, 110 and 151, as opposed to all 256.

The ISPDT depicted in Figure 3 is quite simple. In general, for more complex applications, there may be more elaborate conditionality — for instance, depending upon what is sensed in the first few frames, different choices may be required for subsequent sensing. Such a tree results in multiple target leaves and requires *dynamic* programmability of the sensor.

#### 4. Results

We present successful detection/localization results on the vehicle imagery test data  $I_t$ ,  $t = 0, 1, 3, 4$ , described above, using the ISPDT trained on  $I_2$  and depicted in Figure 3 and Equation 1.

There is no vehicle present at time  $t = 0$ , and (see Figure 4) no pixels fall into the “target leaf”. This implies no detection, as desired.

For  $t = 1, 3, 4$  there is a vehicle present, and (see Figures 5, 6, 7) in each case the existence of pixels falling into the “target leaf” implies detection, as desired. Furthermore, the spatial location of these pixels indicates that the detection is indeed “on target”.

*Remark:* The fact that not all target pixels fall to the “target leaf” is inconsequential; the goal is detection and localization, and in each test case pixels on target are identified ( $t = 1, 3, 4$ ) or no pixels are identified ( $t = 0$ ) as desired.

#### 4.4. Additional Illustration

Figure 8 depicts a more elaborate ISPDT, requiring non-trivial conditioning/adaptation, generated for  $I_3$ . In this tree, as before, Hadamard frame 110 is used at the root, and in the middle cluster at level two Hadamard frame 151 provides clustering into two clusters. While the “target leaf” — the left-most node at level three — provides target detection, there are a significant number of target pixels that fall to the right-most node at level three — a non-target node.

When training on  $I_2$ , tree-building stops at this point. If training on  $I_3$  (presented in Figure 8) it is preferable to continue the tree-building, using Hadamard frame 145 for additional accuracy. Thus the left-most node at level four is an additional “target leaf” for this illustration, and the two target leaves together allow more target pixels to be identified (while still yielding no false detections). This tree would be realized by dynamically programming the sensor to collect Hadamard frame 145 only for cases in which frames 110 and 151 leave detection unresolved.

The scatter plot tree for the illustrative ISPDT depicted in Figure 8 is given in Figure 9. Note that the scatter plots are horizontal location on the  $x$ -axis versus pixel value on the  $y$ -axis. Thus separability of the red (target box) pixels and black pixels is envisioned by projecting onto the  $y$ -axis. For example, initial clustering of Hadamard frame 110 (the root node) produces the three nodes depicted in row two of the figure. These nodes are still depicting frame 110, as at the root. Notice that the target pixels in the middle cluster do not separate from non-target pixels. However, Hadamard frame 151 (the next node in the tree) for these same pixels does provide significant separability.

## 5. Conclusions and Discussion

We have successfully applied ISPDT to DMA hyperspectral imagery for detection/localization, demonstrating the potential of an integrated sensing/processing suite consisting of a dynamically programmable DMA sensor and ISPDT processing.

This example demonstrates detection and localization. When multiple target types are possible, a subsequent classification step — possibly involving additional Hadamard frames, is employed.

If, as is likely in practice, detection is not so “perfect” and some few off-target pixels are identified as falling into the “target leaf” (but still many on-target pixels are so identified) then post-processing under some spatial dependence scheme, such as maximum a posteriori (MAP) spatial filtering, can be used to perform the ultimate detection/localization.

Finally, while it may seem (and is indeed the case) that processing more elaborate than our individual pixel-based approach (such as the use of an edge detector) would make the detection and localization task trivial, the extremely time-sensitive nature of the pattern

recognition applications envisioned here preclude elaborate processing schemes.

## Acknowledgments

Work supported in part by the Applied and Computational Mathematics Program (ACMP) of the Defense Advanced Research Projects Agency (DARPA).

## References

1. C.E. Priebe, D.J. Marchette, and D.M. Healy, "Integrated Sensing and Processing Decision Trees," *IEEE Trans. Pattern Analysis and Machine Intelligence*, 26 (6), 699–708 (2004).
2. R.A. DeVerse, R.R. Coifman, A.C. Coppi, W.G. Fateley, F. Geshwind, R.M. Hammaker, S. Valenti, F.J. Warner, and G.L. Davis, "Application of spatial light modulators for new modalities in spectrometry and imaging," *Proc. SPIE* 4959, 12–22 (2003).
3. M. Harwit and N.J.A. Sloane, *Hadamard Transform Optics* (Academic Press, New York, 1979).
4. R.A. DeVerse, R.M. Hammaker, and W.G. Fately, "Realization of the Hadamard multiplex Advantage Using a Programmable Optical Mask in a Dispersive Flat-Field Near-Infrared Spectrometer," *Applied Spectroscopy*, 54 (12), 1751–1758 (2000).
5. A. Wuttig, R. Riesenbergs, "Sensitive Hadamard Transform Imaging Spectrometer with a simple MEMS," *Proc. SPIE* 4881, 167–178 (2003).
6. L. Hubert and P. Arabie, "Comparing partitions," *Journal of Classification*, 2 193–218 (1985).
7. W.M. Rand, "Objective criteria for the evaluation of clustering methods," *Journal of the American Statistical Association*, 66 846–850 (1971).
8. C. Fraley and A.E. Raftery, "Model-based clustering, discriminant analysis, and density estimation," *Journal of the American Statistical Association*, 97 611–631 (2002).



Fig. 1. Hadamard frame 110 (full  $256 \times 256$  image) for  $I_2$ . T2FP110-256x256.eps



Fig. 2. Hadamard frame 110 ( $64 \times 210$  swath) for  $I_2$ , with target box used for training. T2FP110-64x210.eps

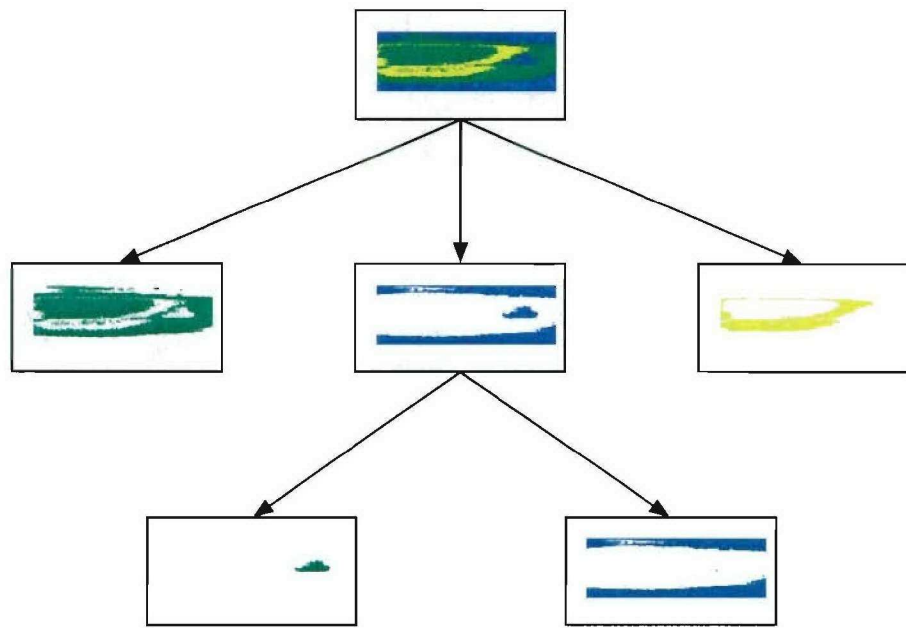


Fig. 3. ISPDT constructed on  $I_2$  (training). The left-most node at level three of the tree is the “target leaf”. psstreeT2.eps

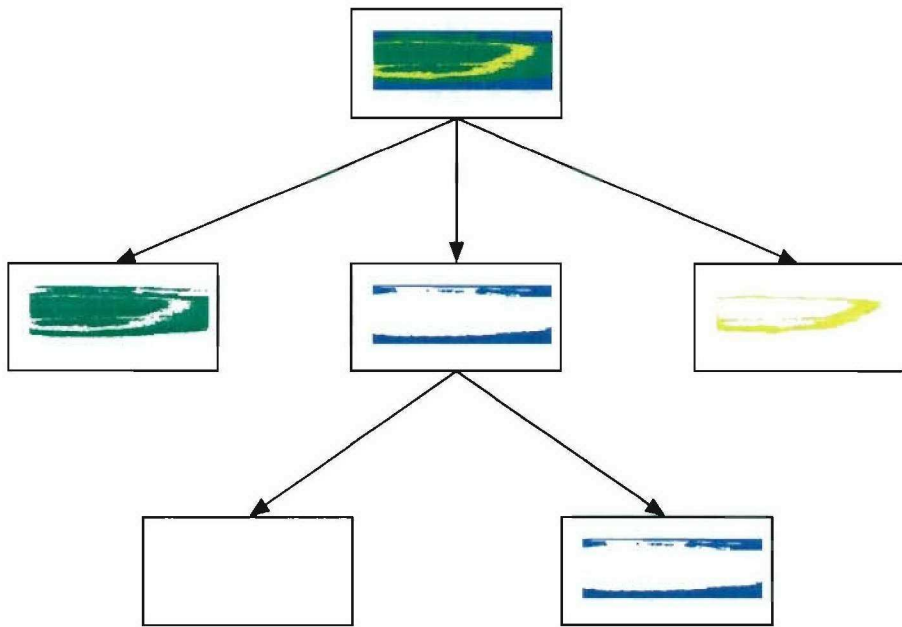


Fig. 4. ISPDT detection/localization results for  $I_0$  (testing). No vehicle is present at time  $t = 0$ , and no pixels falling into the “target leaf” implies no detection, as desired. psstreeT0.eps

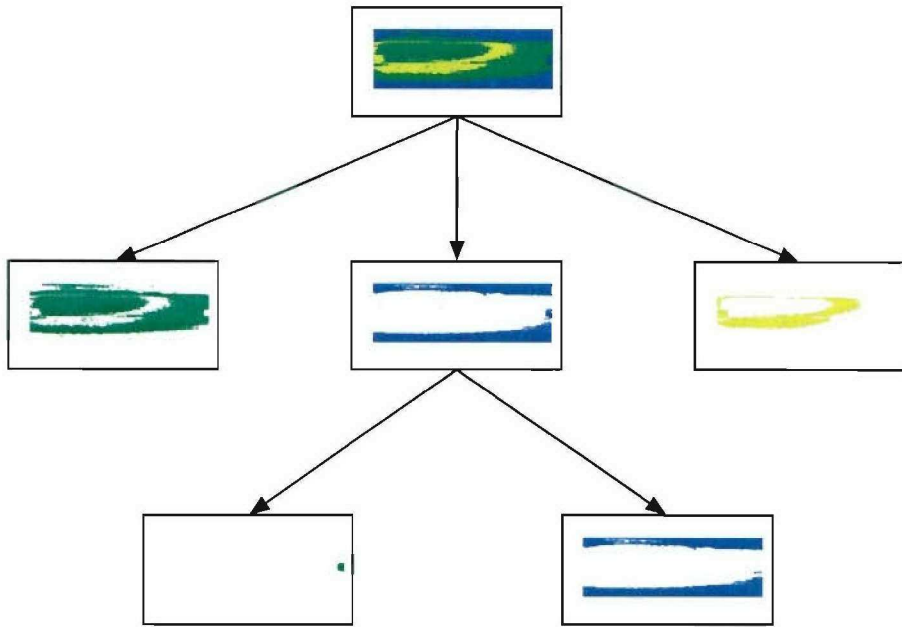


Fig. 5. ISPDT detection/localization results for  $I_1$  (testing). There is a vehicle present at time  $t = 1$ , and the existence of pixels falling into the “target leaf” implies detection, as desired. The spatial location of these pixels indicates that the detection is indeed “on target”. psstreeT1.eps

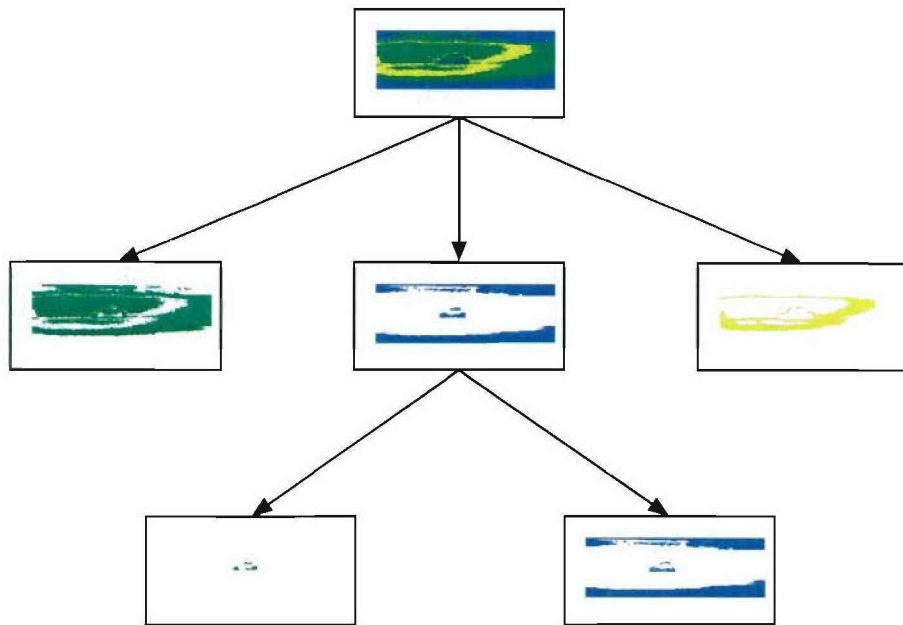


Fig. 6. ISPDT detection/localization results for  $I_3$  (testing). There is a vehicle present at time  $t = 3$ , and the existence of pixels falling into the “target leaf” implies detection, as desired. The spatial location of these pixels indicates that the detection is indeed “on target”. psstreeT3.eps

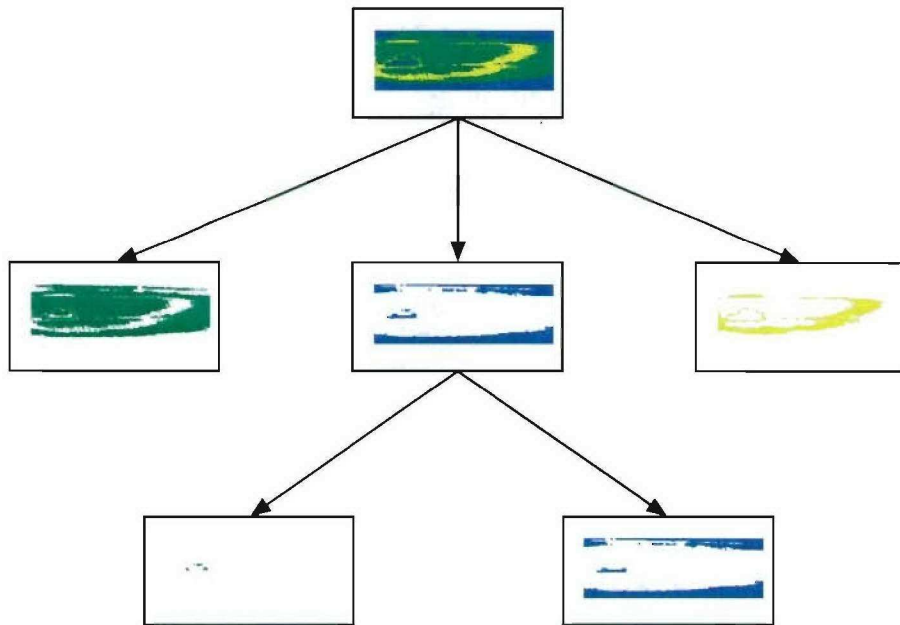


Fig. 7. ISPDT detection/localization results for  $I_4$  (testing). There is a vehicle present at time  $t = 4$ , and the existence of pixels falling into the “target leaf” implies detection, as desired. The spatial location of these pixels indicates that the detection is indeed “on target”. psstreeT4.eps

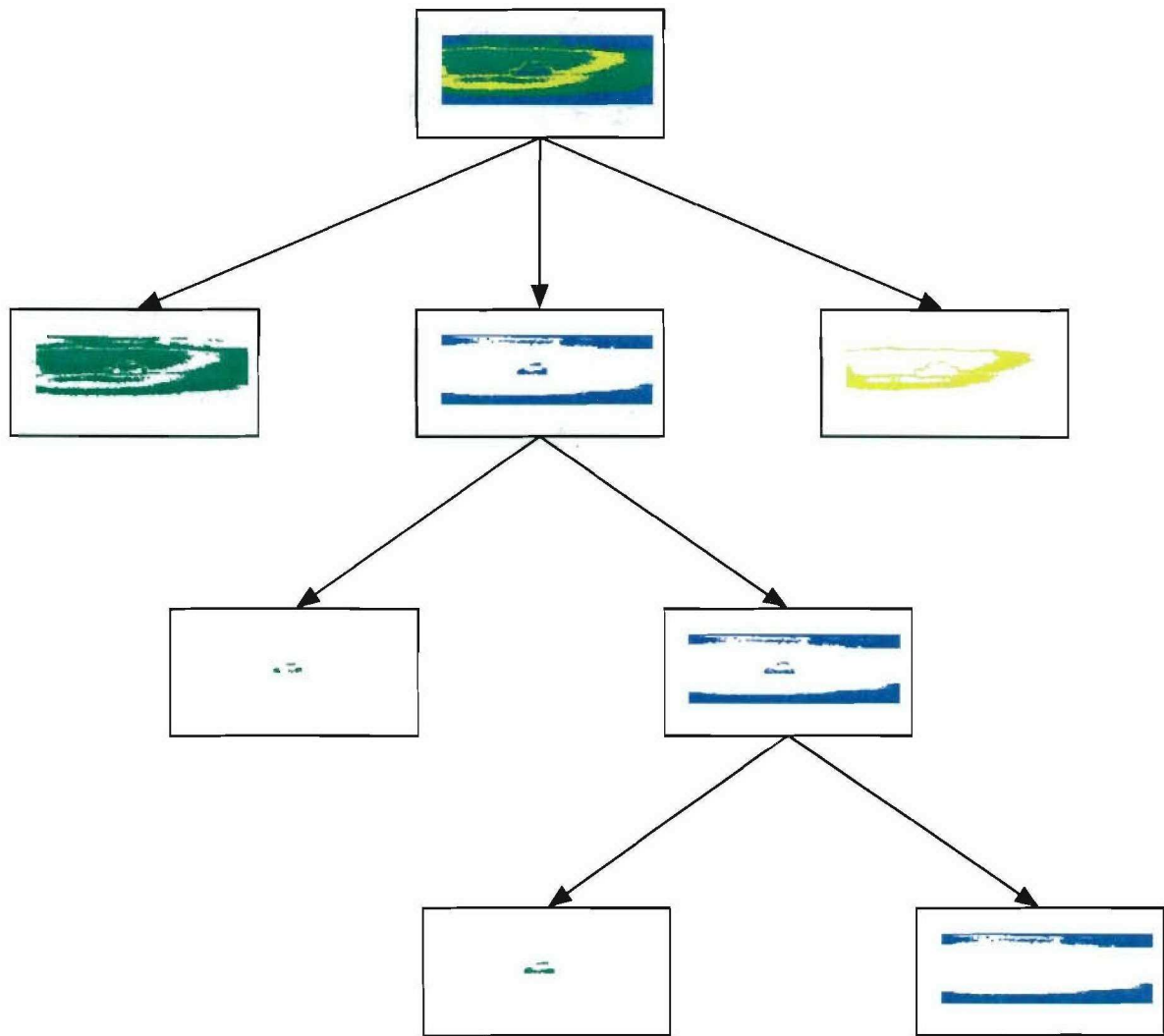


Fig. 8. Illustration of a more elaborate ISPDT, requiring non-trivial conditioning/adaptation, for  $I_3$ . psstreeT3-2.eps

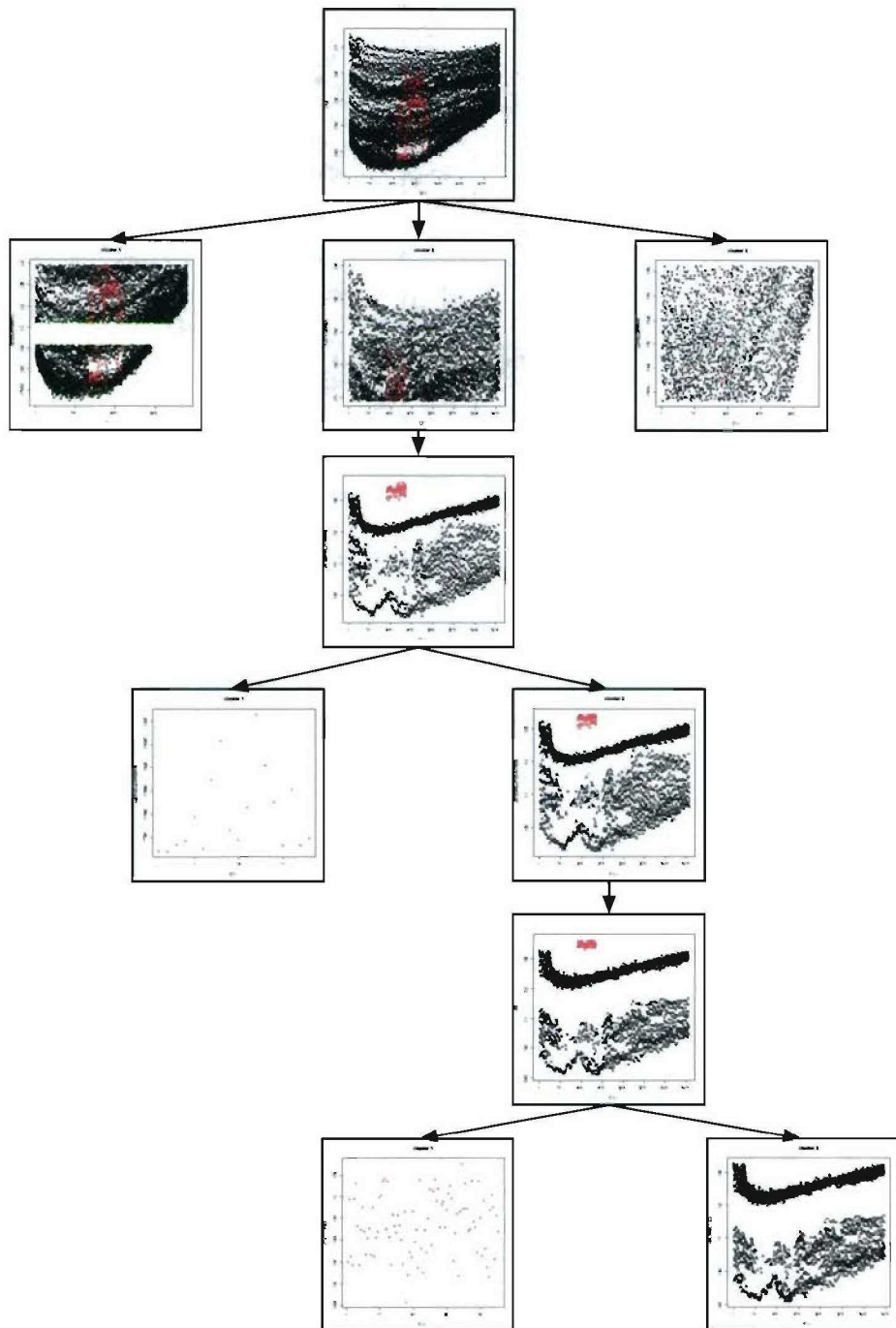


Fig. 9. Scatter plot tree for the illustrative ISPDT depicted in Figure 8. See text for description. psscatterT3.eps